

# Hygrothermal Performance of Multilayer Wall Assemblies Incorporating Starch/Beetpulp in France

*Elias Harb<sup>1</sup>, Chadi Maalouf<sup>1</sup>, Christophe Bliard<sup>2</sup>, Elias Kinab<sup>3</sup>, Mohammed Lachi<sup>1</sup>, Guillaume Polidori<sup>1</sup>*

<sup>1</sup>Laboratoire de MATériaux et Ingénierie Mécanique, <sup>MATIM</sup>, Université de Reims-Champagne-Ardenne URCA, Moulin de la Housse, 51687 Reims Cedex 2, France

<sup>2</sup>Institut de Chimie Moléculaire de Reims, ICMR-UMR 7312 CNRS, Université de Reims-Champagne-Ardenne URCA, Moulin de la Housse, 51687 Reims Cedex 2, France

<sup>3</sup>Université Libanaise, Faculté de Génie, Branche II, Roumieh, Liban

## Abstract

This work focuses, on the investigation of the hygrothermal performance of four different wall insulation assemblies including starch/beet pulp composite in an office in France under two climatic conditions. A comparative performance analysis is made with hemp concrete (HC).

For each design, the overall energy performance, total water content, drying rate and condensation risk were evaluated through hygrothermal simulations using the WUFI® Plus software and mould growth risk assessment was conducted with WUFI®Bio software.

Results showed that insulation assemblies based on S/BP exhibited a superior effectiveness in potential energy savings and higher dryness rate while having a higher condensation risk, a lower dynamic thermal performance, and a higher susceptibility to mould growth risk. Moreover, insulation assemblies based on S/BP demonstrated superior hygrothermal performance under Nancy's climate compared to that of Marseille.

The findings derived from this research enhance the comprehension of the hygrothermal performance exhibited by this innovative bio-composite material and its impact on the overall energy consumption and service performance of a building.

*Keywords: beet-pulp, starch, bio-insulation material, hygrothermal properties, numerical simulation, WUFI®Bio, WUFI® Plus.*

## I. Introduction

Building sector is undoubtedly a massive energy consumer and a main contributor to greenhouse gas emissions across the globe. For instance, at EU level, buildings account for

40% of the total energy consumption and 36% of greenhouse gas emission (European Commission, 2020). While 60% of the total consumed energy in buildings is used for space heating and cooling (Omran et al. 2016), over 50% of energy demand is due to the heat losses through the building envelope and therefore is deemed as a critical element for enhancing buildings thermal performance (Ascione et al. 2019).

Successive thermal regulations (RT 1974, RT1982, RT1988, RT2000, RT2005, RT2012) were introduced in France targeting at first continuous reduction in building energy consumption from 300 kWh/m<sup>2</sup>/year to less than 50 kWh/m<sup>2</sup>/year and lately promoting green constructions (EDF, n.d.). Recently, a new environmental regulation RE2020 in force from January 2022, introduced new environmental standards. It has three main objectives: improving energy performance and furthered reducing energy consumptions in new buildings, reducing carbon footprint and global emissions of new buildings and finally guaranteeing comfort in hot weather as heat waves are expected to become increasingly frequent (Ministère de la transition écologique, 2023).

Although thermal properties of insulation materials and building envelope are crucial for energy saving, hygroscopic properties must be also studied carefully for having a primordial role in controlling and regulating indoor relative humidity levels inside the building.

Uncontrolled levels of relative humidities affect indoor air quality, skin humidity, warm respiratory comfort and can also have a significant impact on energy consumption and building envelope degradation (Xue et al. 2022). Human thermal comfort, cognitive and work performance are closely linked to Indoor Environmental Quality (IEQ) (Li et al. 2023). Relative humidities lower than 30% were associated with increased risk of respiratory diseases (Angelon-Gaetz et al. 2016). Damp and high levels of relative humidity (RH) typically above 70–80% promote an increased risk of mould growth. Exposure to indoor mould contamination has been associated with an increased risk of developing and/or exacerbating a range of allergic and non-allergic diseases (Menneer et al. 2022).

Moreover, Accumulation of moisture in hygroscopic materials can increase their heat conductivity leading to lower energy-saving potential and can cause mould growth and deterioration of artifacts and buildings. Moon & coll. (2014) found that ignoring moisture transfer contributes to a significant error in the measurement of indoor humidity and an

increase in energy consumption by up to 4.4% energy consumption can be obtained when effects of moisture are considered.

Currently, building materials for thermal insulation can be primarily categorized into three types based on their origin, chemical substance and availability: conventional, state-of-the-art and sustainable (Kumar et al. 2020). In his research, he made a comparative analysis of various kinds and performances of building insulation material properties (thermal, hygroscopic, acoustic, reaction to fire, environmental and cost) in different climate zones and proposed an optimization framework based on energy, environment, economic and comfort. Moreover, his analysis showed that walls with higher thermal resistance are less cost-effective for regions requiring more cooling and that insulated and airtight houses may also lead to an increased overheating risk during a hot summer.

However, the rising concerns over climate change and the nearly depletion of non-renewable energy resources have driven the urge of decarbonization of the building sector, the largest energy consumer in France. In conformity with the EU regulation n° 305/2011, bio-based materials concept was introduced in France in the decree of December 19, 2012 defining the content and the conditions of attribution of the “bio-based building” label. As of the 21st century, the bio-insulating material identified as low-embodied energy materials that reduce energy use and greenhouse gas emissions sector, has experienced relatively recent development in France (Rabbat et al. 2022). For this matter, many researches have focused on designing and testing various insulation materials made from renewable biomass resources and wastes for building insulation use.

In this context, Badouard & coll. (2021) investigated the development and characterization of new bio-based materials based on viticulture by-products and potato starch for building insulation use. Jerman & coll. (2019) investigated the hygrothermal properties of five biomaterials (Wood fibreboard, flax fibres, hemp fibres, jute fibres, and sheep wool suitable) potentially applicable in interior thermal insulation systems suitable for historical and traditional buildings. Zhou & coll. (2023) investigated the influence of fibre size, binder type and binder ratio on the hygrothermal properties of insulation materials made from rice straw and natural binders.

Moreover, in order to conduct these investigations, various heat and moisture transfer models have demonstrated notable efficacy in examining the hygrothermal performances of insulation materials. Among them WUFI® software proved to be a powerful hygrothermal simulation software based on the model developed by Kunzel (Kunzel, 1995). It has complied with the general requirements of standards DIN EN 15026:2007 (IBP, 2007) besides being used and experimentally validated over the years by researchers (Lee et al. 2020) (Tlaji et al. 2022) (Feng et al. 2022).

Liuzzi & coll. (2017) investigated hygrothermal properties of several clayey materials incorporating different percentages of leaves and small branches derived from the pruning of olive trees. Simon & coll. (2021) investigated hygrothermal and mechanical performance of different sustainable concrete mix designs. Coelho & coll. (2018) validated hygrothermal simulation models for historical buildings while taking into consideration most of the processes that affected the hygrothermal performances.

Nevertheless, the process of hygrothermal performances evaluation involved study of various risks under different climates for building construction materials (e.g. total water content, drying rate, condensation, mould growth ...). Careful examination of such risks is considered crucial for avoiding any potential damage in building envelope/structure and health hazards.

In this regard, Ho Ryu & coll. (2015) evaluated the influence of hygric properties of various wallpapers on mould growth rates using hygrothermal simulation. Brambilla & coll. (2020) investigated condensation and mould growth risk through hygrothermal simulations in timber-based wall assemblies. Tlaji & coll. (2022) investigated total water content, drying rate, condensation risk, mould growth, moisture quantity, time lag and decrement factor of various multi-layered straw walls with different boundary conditions. Results showed that wall's performance strongly depended on the interior and exterior added thermal insulation layers as they affected the ability of the material to dry out. Xue & coll. (2022) investigated moisture accumulation in building envelopes and its influences on condensation and mould growth. Results showed that moisture content as well as condensation and mould risk are closely related to the building wall orientation.

Furthermore, various researchers investigated a new bio-composite material based on beet pulps derived from sugar extraction process from sugar beets and potato starch for

building insulation use at material and wall scale. Mechanical, hygrothermal and acoustical studies on this novel material revealed promising results. In this context, Karaky (2018) studied during his PhD physical properties (morphology, porosity, density and particles size), mechanical and acoustical performance of starch/Beet pulp bio composite. A mass ratio equal to 0.4 was found to be the optimal composition of S/BP in terms of the hygrothermal and mechanical properties. Costantine & coll. (2020) compared the drying kinetics and mechanical properties of whole vs. hollowed S/BP bricks having similar mixture composition. Harb & coll. (2023) studied the thermal performance of S/BP composite for building insulation at a wall scale. Tenpierik & coll. (2023) investigated the thermal inertia of S/BP bricks enhanced with phase change materials.

Based on the above findings, the aim of this paper is to elaborate at first thermal and hygric properties of S/BP bio-composite that do not exist in literature. Afterwards, an evaluation of the hygrothermal and bio-hygrothermal performances of insulation assemblies made of Starch/Beet pulp, were conducted using the WUFI® PLUS and WUFI®bio softwares, respectively. This assessment entailed a comparative analysis with insulation assemblies made of hemp concrete, under the climatic conditions of two distinct cities in France - Nancy and Marseille. For this purpose, a renovation case study was adopted for an existing office (6m x 5m x 3m) under Nancy's climate conditions in France. Insulation walls made of S/BP were attached to the interior side of office walls made of clay bricks. Various insulation wall designs were studied.

For each design, the overall energy performance, total water content, drying rate, condensation risk was evaluated. In a final step, the software WUFI®-bio was used to evaluate the potential mould risk based on the obtained simulation results from WUFI® PLUS software.

## **II. Experimental set-up and Methodology**

### ***II.1 Material assembly***

In this study, the elaboration of starch/beet pulp bio-composite was conducted using a similar methodology as described by Costantine & coll. (2020) while adhering to a mass ratio of 0.4.

This mass ratio has demonstrated his ability to yield optimal results in terms of mechanical, acoustical and hygrothermal performances (Karaky et al. 2018) (Karaky et al. 2019).

In accordance with the aforementioned fabrication procedure, dry beet pulps were totally submerged in water with a mass ratio of water to beet pulp set equal to 2.5. This immersion lasted for a duration of 2 hours until complete saturation was achieved. Subsequently, manual mixing of potato starch with the saturated wet pulps took place for a period of 10 minutes to ensure thorough homogenization. The mixture was introduced into an autoclave, ensuring a controlled heating at a temperature of 120 °C for a duration of 30 minutes. Afterwards, Starch/beet-pulp samples were obtained by pouring the mixture into wooden moulds and subsequently subjecting it to mechanical compaction at a pressure of 0.044 MPa. In the final step, samples were frozen at -80°C then dried using a freeze-dryer. This drying method resulted in a minimal shrinkage percentage of 2.5% while maintaining a superior surface quality of the samples compared to pulsed hot air drying.

## **II.2 Water Vapour permeability**

The water vapour permeability  $\delta m$  (kg/m.s.Pa) describes the ability of a material to transfer moisture under a gradient of vapour pressure.

During his PHD studies, Karaky (2018) performed the “dry cup” test for lower humidities conditions on various Starch-Beet Pulp (S/BP) Composites according to the European standard NF EN ISO 12572:2016. Water vapour permeability and water vapour resistance factor were obtained respectively equal  $6.98 \pm 0.246 \times 10^{-12}$  kg/m.s.Pa and  $28,67 \pm 1.02$  for a S/BP composite with a mass ratio of equal to 40%. In this study, the water vapour permeability was measured by using the “wet cup” method for higher humidities conditions as described in the same standard.

For this purpose, five cylindrical S/BP samples ( $D = 0.09$  m,  $H = 0.03$  m) were elaborated. They were placed for two weeks inside a climatic chamber Binder MKF 720 conditioned at 50% RH and 23 °C until mass stabilization.

Afterwards, the sides of the specimens were sealed with waterproof aluminum tape, and then each specimen was fixed at the top of a cup enclosing at its bottom a solution of potassium nitrate ( $KNO_3$ ) in order to ensure an inside relative humidity of around  $94 \pm 1\%$ . Finally, all specimens were placed inside the climatic chamber Binder MKF 720, as shown in Fig. 1. The

air space  $da$  (m) between the saturated solution and the specimen was maintained equal to 0.015 m for all tests.

In order to eliminate the resistance of the air layer above the specimens, an air velocity exceeding 2 m/s was ensured on the top surface of the cups. Cups were regularly weighed by using an analytical balance with 0.001 g resolution every 48 hours until a steady state was reached.



**Figure 1 : S/BP samples having their sides sealed with waterproof aluminum tape and fixed at top of cups enclosing a solution of potassium nitrate (KNO<sub>3</sub>) at their bottoms**

The density of water vapour flow rate  $g$  (kg/m<sup>2</sup>.s) through a sample was determined by Eq. (1) and Eq. (2):

$$\Delta\dot{m}_{12} = \frac{m_2 - m_1}{t} \quad (1)$$

$$g = \frac{G}{A} \quad (2)$$

where  $G$  (kg/s) is the mean value of five successive determinations of  $\Delta\dot{m}_{12}$  for each specimen (kg/s) and  $A$ (m<sup>2</sup>) is the Exposed area of the test specimen.

Since the S/BP composite is a highly permeable material, the resistance of the air gap between the base of the sample and the saturated solution of potassium nitrate (KNO<sub>3</sub>) was considered

in the calculation. The corrected vapour permeance  $W$  (kg/m<sup>2</sup>.s.Pa) and the water vapour resistance  $Z$  (m<sup>2</sup>.s.Pa/Kg) were determined by Eq. (3) and Eq. (4) respectively and whereas the water vapour pressure difference across specimen  $\Delta p_v$  (Pa) and the Water vapour permeability of air  $\delta_a$  (kg/m.s.Pa) were considered equal respectively to 1207 Pa and  $2 \times 10^{-10}$  kg/m.s.Pa for a test condition of 23 °C and 50/93 % RH:

$$W = \frac{1}{\frac{A \cdot \Delta p_v}{G} - \frac{d a}{\delta a}} \quad (3)$$

$$Z = \frac{1}{W} \quad (4)$$

Finally ,the water vapour permeability of specimen  $\delta$  (kg/m.s.Pa),the water vapour resistance factor  $\mu$  and the water vapour diffusion-equivalent air layer thickness  $Sd$  (m) were determined respectively by Eq. (5) to Eq. (7) :

$$\delta = W \cdot d \quad (5)$$

$$\mu = \frac{\delta_a}{\delta} \quad (6)$$

$$Sd = \mu \cdot d \quad (7)$$

Where,  $d$ (m) is the specimen thickness.

### **II.3 Capillary absorption coefficient**

The capillary absorption coefficient refers to the capacity of an insulation material to absorb water when only a portion of its surface is exposed for a short time. As a result, the material's ability to withstand water infiltration into its structure under conditions such as direct exposure to driving rain can be identified.

This coefficient is important for insulation materials, as excessive water absorption can lead to a reduction in their insulating properties and may also cause the material to deteriorate over time. Insulation materials with a low coefficient of water absorption by partial immersion are therefore preferred for applications where moisture resistance is important.



Therefore, the water absorption coefficient value  $A_w$  ( $\text{Kg}/\text{m}^2 \cdot \text{S}^{0.5}$ ) is thus expressed as the mass of water absorbed by a test specimen per face area  $\Delta m_t$  ( $\text{Kg}/\text{m}^2$ ) per square root of time and is determined by a one-directional free water intake test at least for 24 hours according to the European standard NF EN ISO 15148 as described by Eq. (8) and Eq. (9):

$$\Delta m_t = \frac{m_t - m_i}{A} \quad (8)$$

$$A_w = \frac{\Delta m_t}{\sqrt{t}} \quad (9)$$

For this purpose, four identical S/BP bricks ( $L = 0.2185$  m,  $t = 0.103$  m and  $H = 0.056$  m) were elaborated. Bricks were placed for two weeks inside a climatic chamber Binder MKF 720 conditioned at 50% RH and 23 °C. After mass stabilization, each brick was weighed with a balance capable of weighing test specimens to an accuracy of  $\pm 0.1\%$  in order to determine their initial weights  $m_i$ . The sides of bricks were sealed with waterproof aluminium tape in order to ensure one dimensional water flow.

Then they were placed inside a tank on point supports to keep it clear from bottom. The tank was partially filled with water conditioned at 23 °C until it reached 5 mm higher than the submerged base of the specimen placed inside the tank. The water level was maintained on this level  $\pm 2$  mm during the entire test. Each brick was weighted after 1,3,5,7,10,15,20,30,60,120,1440 minutes.

#### ***II.4 Moisture content at free saturation***

The moisture content at free saturation for insulation materials refers to the highest amount of water that a material can freely absorb when totally submerged in water for a long time without vacuum. It is defined in literature by the long-term water absorption by total immersion coefficient  $W_{lt}$  (volume percent) or by the free water saturation coefficient  $W_f$  ( $\text{kg}/\text{m}^3$ ).

For bio-composites materials,  $W_{lt}$  depends on various factors such as the type and amount of natural fibres used, the type of binder and the manufacturing process. The determination of this coefficient is inevitable for bio composites materials as water saturation can compromise

the insulating properties effectiveness and potentially affect the mechanical properties by weakening the natural fibres and leading to dimensional changes or even structural damage.

In this study, Wlt was determined in a free water intake test by totally immersing S/BP bricks in water according to Method 2A (long-term water absorption by total immersion - drainage) listed in the European standard NF EN ISO 16535:2019.

For this purpose, four identical S/BP bricks (L = 0.2185 m, t = 0.103 m and H= 0.056 m) were elaborated and were placed for two weeks inside a climatic chamber Binder MKF 720 conditioned at 50% RH and 23 °C.

Afterwards, each brick was placed inside an empty tank. A sufficient point load was applied to it in order to keep the tested specimen totally immersed in water while maintaining the slightest contact possible with the load.

In a later step, the tank was filled with water conditioned at 23 °C until the top face of the test specimen is (50 ± 2 mm) submerged below the surface of the water. The water level was maintained on this level during the entire test.

Long-term water absorption by total immersion Wlt (%) and Wf (kg/m<sup>3</sup>) were determined based on the total water absorbed after saturation by Eq. (10) and Eq. (11) respectively:

$$Wlt = \frac{mt - mi}{V} \times \frac{100}{\rho_w} \quad (10)$$

$$Wf = \frac{mt - mi}{V} \quad (11)$$

Where, V (m<sup>3</sup>) is the volume of the test specimen and  $\rho_w$  (kg/m<sup>3</sup>) is the density of water.

### ***II.5 Thermal conductivity***

In their study, Karaky & coll. (2019) examined the thermal conductivity of S/BP at an ambient temperature of 20 °C and a relative humidity of 10 %. Under these specific conditions,

the thermal conductivity of this bio-composite for a mass ratio equal to 0.4 was determined equal to  $0.0757 \text{ W}/(\text{m}\cdot\text{K})$ .

In order to furtherly investigate the correlation between thermal conductivity and relative humidity, thermal conductivity tests were carried out on three identical S/BP bricks ( $L = 0.1 \text{ m}$ ,  $t = 0.1 \text{ m}$  and  $H = 0.1 \text{ m}$ ) regulated for two weeks at an ambient temperature of  $20 \text{ }^\circ\text{C}$  and a relative humidity of 60 %. The thermal conductivities were measured using an Isomet 2114 (Applied Precision) device, which employs a dynamic measurement method to reduce the measurement time in comparison with steady state measurement methods. The heat flow is produced by an electrical heating of resistor heating in direct contact with the tested sample. The assessment of thermal conductivity is performed by periodically recording the sampled temperature as a function of the time. The measurement reproducibility of the device was  $3\% + 0.001 \text{ W}/(\text{m}\cdot\text{K})$ .

### **III. Numerical simulation**

#### ***III.1 Case study***

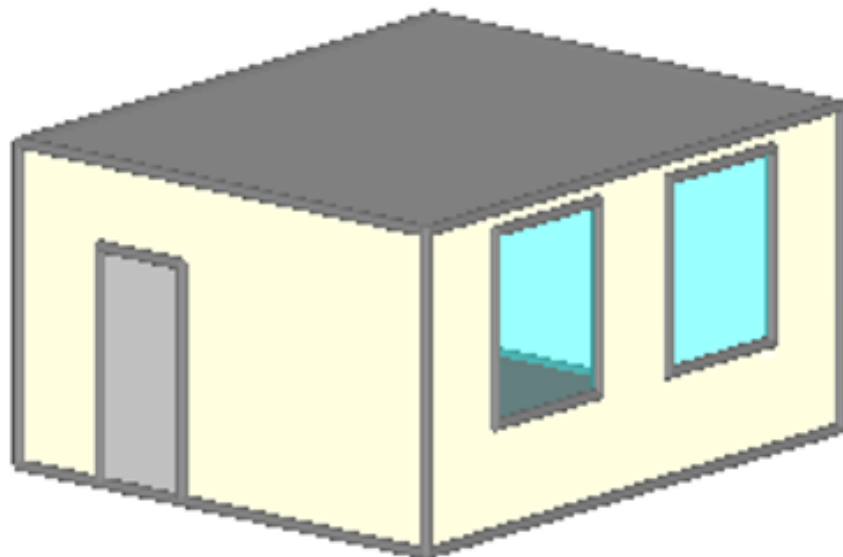
It is important to note that the S/Bp bio-composite material is not intended for use as a structural building material, and should not be exposed to very high levels of humidity under normal use. Rather, It is designed to be installed as interior insulation within the building envelope.

For the purpose of this study, hygrothermal and bio-hygrothermal studies were conducted to examine the performance of four different insulation assemblies made of S/BP. These investigations involved altering the thickness of starch/beet pulp bio-composite and incorporating various air layers as described in table 1. In order to evaluate the hygrothermal and bio-hygrothermal performances of these assemblies, a simplified one-story office building ( $6\text{m} \times 5\text{m} \times 3\text{m}$ ) was modelled in WUFI® Plus as shown in Fig. 2. This software showed to be the most complete heat and moisture simulation tool in the WUFI® software family. In addition to simulating hygrothermal conditions of different building components, it is suitable for addressing energy consumption and comfort in buildings. Consequently, poor performance and/or damage can be avoided in building design phase (e.g., summer overheating, mould, etc. ...) (WUFI®, 2019) .

The purpose of this simulation is to evaluate the viability of these assemblies as internal insulation for office walls constructed with aerated clay brick, under two distinct climatic conditions in France, namely the cities of Nancy and Marseille. Subsequently, a comparative performance analysis is made between the S/BP bio-composite and hemp concrete for the four different assemblies used in this study under Nancy's climate.

For each case the overall energy performance, total water content, drying rate, condensation risk, mould growth, time lag and decrement factor were evaluated through the numerical simulations.

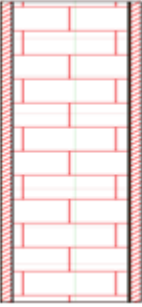
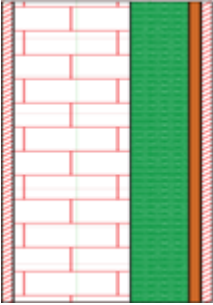
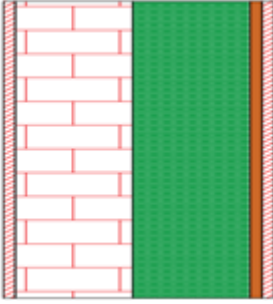
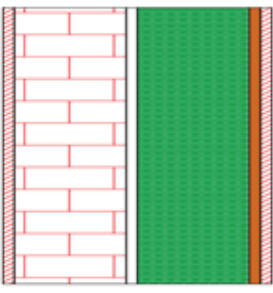
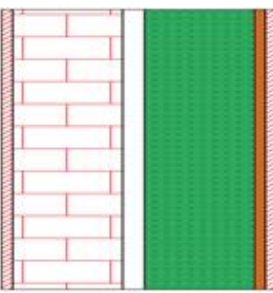
The outer temperature and relative humidity, sun radiation and driving rain informations for the French cities of Nancy and Marseille were acquired from the built-in database within the WUFI® Plus program and are shown in Fig. 3 to Fig. 6 respectively.



**Figure 2 : Schematic representation of the office under investigation**

### **Table 1**

Different insulation wall assemblies of five considered cases.

Case		Wall assembly design					
		Layer 1	Layer 2	Layer 3	Layer 4	Layer 5	Layer 6
(0)		Exterior plaster (2 cm)	Clay brick (20 cm)	Interior plaster (2 cm)	-	-	-
(a)		Exterior plaster (2 cm)	Clay brick (20 cm)	S/BP (10 cm)	Hardwood (2 cm)	Interior plaster (2 cm)	-
(b)		Exterior plaster (2 cm)	Clay brick (20 cm)	S/BP (20 cm)	Hardwood (2 cm)	Interior plaster (2 cm)	-
(c)		Exterior plaster (2 cm)	Clay brick (20 cm)	Air layer (2 cm)	S/BP (20 cm)	Hardwood (2 cm)	Interior plaster (2 cm)
(d)		Exterior plaster (2 cm)	Clay brick (20 cm)	Air layer (4 cm)	S/BP (20 cm)	Hardwood (2 cm)	Interior plaster (2 cm)

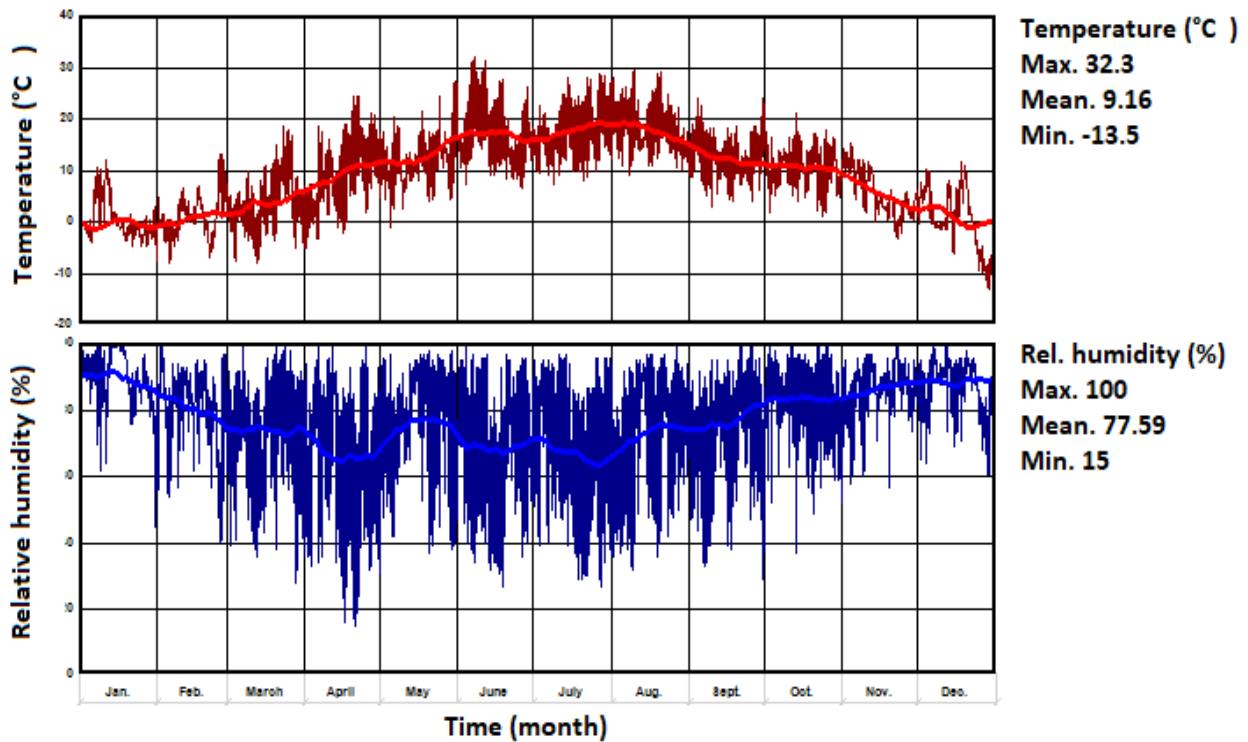


Figure 3 : Outer temperature and relative humidity information obtained from WUFI®plus for Nancy's climate

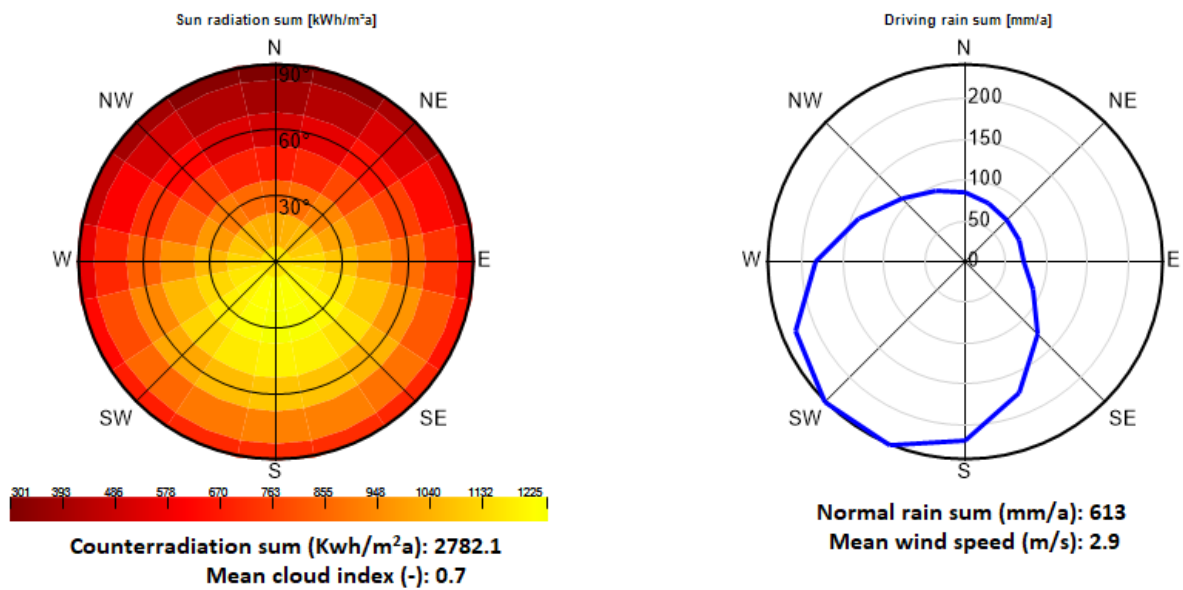


Figure 4 : Sun radiation and driving rain information obtained from WUFI®plus for Nancy's climate

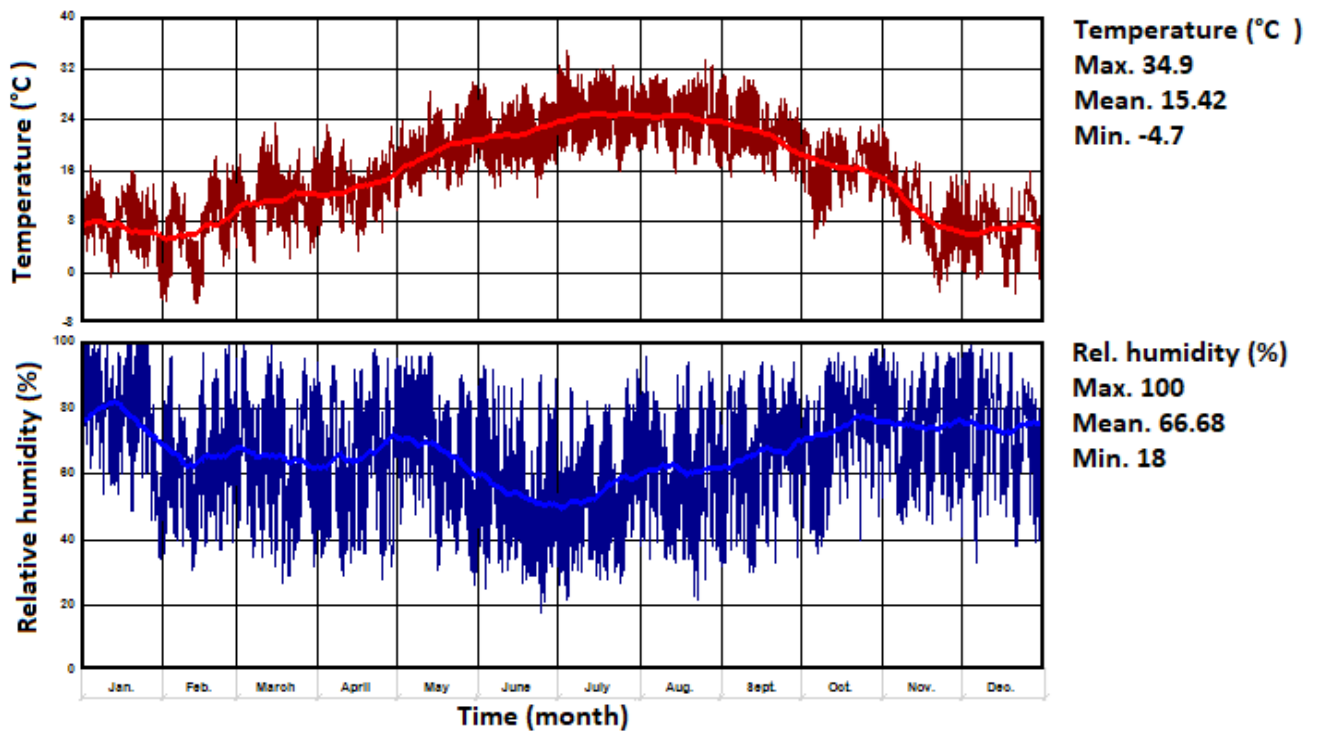


Figure 5 : Outer temperature and relative humidity information obtained from WUFI®plus for Marseille’s climate

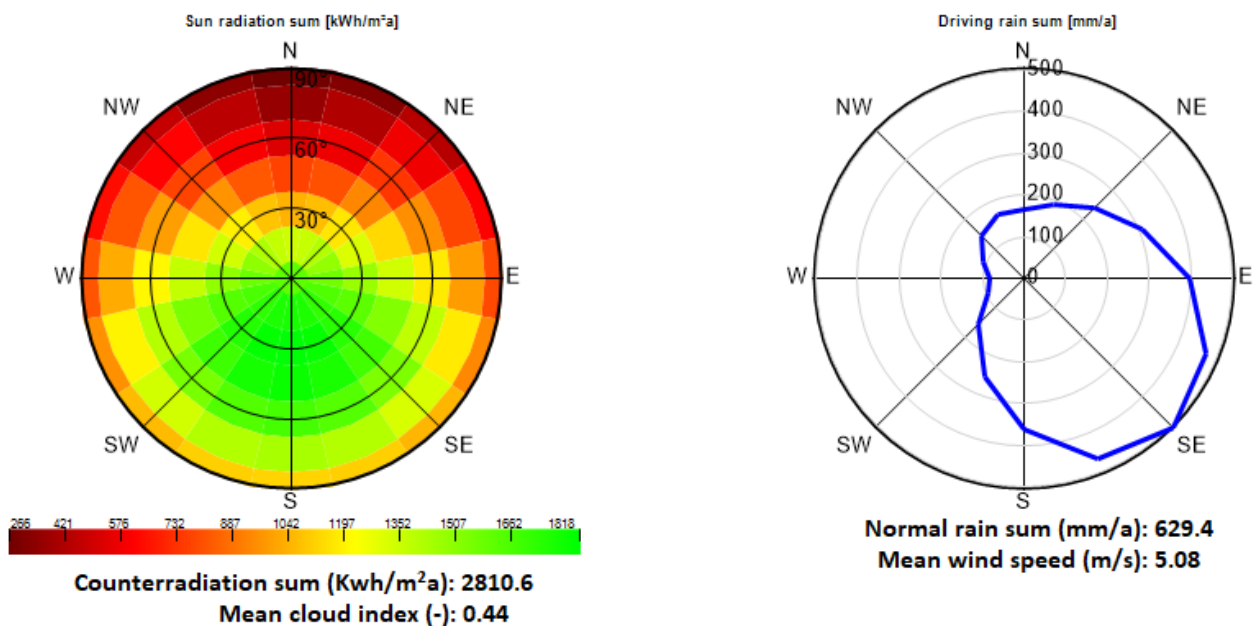


Figure 6 : Sun radiation and driving rain information obtained from WUFI®plus for Marseille’s climate

### III.2 Hygrothermal simulation

A numerical model based on WUFI®plus software is used to predict the hygrothermal response of the S/BP wall assemblies under different weather conditions. It was developed by

the Fraunhofer Institute for Building Physics (Germany) and is based on solving the coupled heat and moisture transfer models proposed by Künzle (1995) as shown in in Eqs. (12) and (13):

$$\left( \rho c + \frac{\partial H_w}{\partial \theta} \right) \cdot \frac{\partial \theta}{\partial t} = \nabla \cdot (\lambda \Delta \theta) + h_v \nabla \cdot (\partial p \nabla (\phi P_{sat})) \quad (12)$$

$$\frac{\partial w}{\partial \phi} \cdot \frac{\partial \phi}{\partial t} = \nabla \cdot (D_l \cdot \frac{\partial w}{\partial \phi} \nabla \phi) + \partial p \nabla (\phi P_{sat}) \quad (13)$$

where  $\rho$ ,  $c$  are respectively the bulk density ( $\text{kg}/\text{m}^3$ ) and the specific heat ( $\text{J}/(\text{kg}\cdot\text{K})$ ) of the dry material and  $H_w$ ,  $\theta$ ,  $t$ ,  $\lambda$ ,  $h_v$ ,  $\delta p$ ,  $\phi$ ,  $P_{sat}$ ,  $w$  and  $D_l$  are respectively the enthalpy of water ( $\text{J}/\text{m}^3$ ), the temperature ( $^\circ\text{C}$ ), the time (s), the thermal conductivity ( $\text{W}/(\text{m}\cdot\text{K})$ ), the latent heat of evaporation ( $\text{J}/\text{kg}$ ), the vapour permeability ( $\text{kg}/(\text{m}\cdot\text{s}\cdot\text{Pa})$ ), the relative humidity, the saturation vapour pressure (Pa), the moisture content ( $\text{kg}/\text{m}^3$ ) and the liquid diffusivity ( $\text{m}^2/\text{s}$ ).

The primary mechanism for moisture transport mechanism in capillary porous materials is the capillary liquid transport. This mode of transport can be characterized by two distinct liquid transport coefficients: The liquid transport coefficient for suction  $D_{ws}$  ( $\text{m}^2/\text{s}$ ) and the liquid transport coefficient for redistribution  $D_{ww}$  ( $\text{m}^2/\text{s}$ ).

The  $D_{ws}$  describes the capillary uptake of water by a building facade during exposure to rainfall, wherein the transport is dominated by the larger capillaries. In contrast,  $D_{ww}$  describes the dispersion of absorbed water within the materials after the rain has ceased, with transport will be dominated by the smaller capillaries.

Unfortunately, the aforementioned transport coefficients are difficult to measure for the majority of materials. Reliant on the water content, the liquid transport coefficient for suction  $D_{ws}$  ( $\text{m}^2/\text{s}$ ) and the liquid transport coefficient for redistribution  $D_{ww}$  ( $\text{m}^2/\text{s}$ ) can be estimated by using WUFI® plus software as shown in Eqs. (14) to (16):



$$Dws(w) = 3.8 \cdot \left(\frac{Aw}{wf}\right)^2 \cdot 1000 \left(\frac{w}{wf}\right)^{-1} \quad (14)$$

$$Dww(w80) = Dws(w80) \quad (15)$$

$$Dww(wf) = Dws(wf)/10 \quad (16)$$

Where  $w$  (kg/m<sup>3</sup>) is the moisture content mass by volume,  $w80$  and  $wf$  indicate a moisture content for a relative humidity equal to 80% and 100% respectively.

### **III.3 Materials and design conditions**

Each hygrothermal study was conducted over a duration of four years with a maximum time step results recorded at one-hour intervals. The calculation accuracy was set to very high.

The following design conditions were consistently held constant for all simulations:

At the southern façade, two uncoated double glazed windows were installed, each measuring 1.5 meters in width and 1.8 meters in height. Consequently, the ratio of window area per floor area reached 18%. Additionally, on the Western façade, a wooden door measuring 1 meter in width and 2.2 meters in height was incorporated to the structure.

Given the specific focus of the hygrothermal analysis on evaluating the impact of insulation assemblies on wall components and the overall performance of the system, an assumption was made that the slab and roof experienced no heat or moisture exchange with the external climate. Consequently, both of these components were treated as adiabatic and impermeable materials.

Moreover, due to the fact that the hygrothermal behaviour of a wall is significantly affected by various factors such as solar radiation, driving rain intensity and direction as well as the orientation of the structure, focus is made on north-oriented walls, as this orientation tends to experience higher driving rain intensity and lower solar radiation which amplifies the likelihood of encountering moisture-related issues.

It is assumed that the office building is occupied from 08:00 to 17:00, five days per week with 3 adults working in an office job.

Within the designated occupancy hours, the metabolic rates generated by each individual is listed in table 2, acquired from the built-in database within WUFI®plus software. Moreover, an additional internal load of 200 Watts was presumed for other internal loads originating from lighting fixtures and various office equipment.

To ensure the maintenance of a comfortable and healthy indoor environment, a mechanical ventilation system was established in conjunction with a permanent air infiltration through building leakages. The air change per hour ACH (h<sup>-1</sup>) values were set equal to 1.5 and 0.1 for mechanical ventilation and air infiltration, respectively.

Only temperature was controlled for all designs through a heating and a cooling system. Temperature set points were established at 21°C and 25°C.

Conversely, during non-occupancy hours, no internal loads were generated; the ACH for the mechanical ventilation system was consistently maintained at a value of 0.75. Furthermore, the maximum and minimum temperature set-point values for the cooling and heating systems were set equal to 17 °C and 27 °C, respectively.

Lastly, the hygrothermal characteristics of the building materials used in this study are listed in Table 3, while table 4 presents the moisture storage functions for HC and S/BP.

**Table 2**

Metabolic rate data for one adult/sitting person/working acquired from the built-in database within WUFI®plus software.

Setting	Heat convective (W)	Heat radiant (W)	Moisture (g/hr)	CO2 (g/hr)	Human activity (met)
Adult, sitting person, working	80	41	59	36.3	1.2

**Table 3**

Building materials hygrothermal properties.

Element	$\rho$ (kg/m <sup>3</sup> )	Porosity (-)	Cp (J/kg.K)	$\lambda$ , dry 10 °C (W/m.K)	$\mu$ ,dry (-)	Wf (kg/m <sup>3</sup> )	Aw (kg/m <sup>2</sup> .s <sup>0.5</sup> )	References
Exterior plaster	1310	0.36	850	0.87	8	192	0.001	The database of WUFI®plus software
Aerated clay brick	672	0.67	850	0.12	4	291	0.046	The database of WUFI®plus software

Air layer (2 cm)	1.3	0.999	1000	0.13	0.56	-	-	The database of WUFI®plus software
Air layer (4 cm)	1.3	0.999	1000	0.23	0.38	-	-	The database of WUFI®plus software
S/BP	360	0.706	1410	0.075	28.67	641.59	0.154	This study; Karaky (2018)
Hardwood	650	0.47	1400	0.13	200	-	-	The database of WUFI®plus software
Interior plaster	850	0.65	850	0.2	8.3	400	0.287	The database of WUFI®plus software
Hemp concrete	466	0.78	741	0.0995	2.02	541	0.14	(Seng et al. 2019a); (Seng et al. 2019b)

**Table 4**

Moisture storage function comparison between HC and S/BP.

	RH (%)					References
	20	40	60	80	92	
Water content within HC (Kg/m <sup>3</sup> )	5.65	8.71	12.68	20.32	29.96	Karaky (2018)
Water content within S/BP (Kg/m <sup>3</sup> )	6.16	17.26	31.32	53.02	67.56	Seng & coll. (2019)

### **III.4 Energy Performance**

The impact of each configuration was assessed by evaluating the overall cooling load during summer and heating load during winter.

### **III.5 Hygric evaluation**

Excessive moisture content in building materials can lead to various detrimental effects such as decreased thermal performance, bio-degradation, mould growth and structural decay. Using WUFI®Plus software, detailed predictions were made for the total water content, drying rate and condensation risk criteria. Based on the findings, moisture concerns were identified and highlighted for each configuration.

#### **III.5.1 Total water content**

The total water content TWC refers to the amount of water present within a building material at a specific time for specific environmental conditions. A day-averaged of the total

water content is estimated by the WUFI®Plus software for all scenarios over a span of four years. The variations of the total water content observed throughout these years will indicate whether the material will encounter excessive moisture content or maintain a stable state. This evaluation can be conducted by comparing the initial and the final moisture content. The criterion for passing this assessment is met if the final water content is lower than its initial content.

### **III.5.2 Dryness rate**

The dryness rate measures the ability of a wall to dry out and reduce its moisture content. For each configuration, it is equal to the difference between the total initial water content  $TWC_i$  ( $\text{Kg}/\text{m}^2$ ) and the total final water content  $TWC_f$  ( $\text{Kg}/\text{m}^2$ ) of all layers within the studied assembly divided by its total initial water content over four years as shown in Eq. (17):

$$DR = \frac{TWC_i - TWC_f}{TWC_i} \times 100 \quad (17)$$

A negative rate of DR signifies that the wall is accumulating humidity and moisture over the course of the study period, rendering it highly susceptible to moisture related-issues. Conversely, positive rate indicates that the wall is progressively shredding the humidity. Whereas, higher values of DR reflect a greater ability to eliminate moisture, while lower values indicate a slower rate of moisture reduction.

Subsequently, monitoring the DR is crucial for understanding the overall moisture performance and durability of the building envelope.

### **III.5.3 Condensation risk**

Condensation risk (CR) refers to the potential for water vapour to condensate within the building envelope. This risk can manifest either on the indoor surface or within the wall. Surface condensation occurs when its temperature falls below the dew point temperature within the indoor environment. In such cases, The CR is determined by calculating the percentage of time the surface temperature remains below the dew point.

Within the wall, CR arises when the vapour pressure exceeds the saturated vapour pressure. In this study, the risk was evaluated based on the ASHRAE standard 160P, which prescribes

the criteria for moisture control design and analysis in buildings (ASHRAE, 2008). This standard, which was also employed by Brambilla & coll. (2020), sets three performance criteria aimed at minimizing potential issues related to moisture and mould growth within the building envelope, and in particular:

A. 30-day running average surface relative humidity to be lower than 80%

B. 7-day running average surface relative humidity to be lower than 98%

C. 24-hour running average surface relative humidity to be lower than 100%

Subsequently, The CR within the wall is determined by quantifying the percentage of time during which these criteria were not met.

### **III.6 Dynamic thermal behaviour**

In order to gain a deeper understanding of the dynamic thermal behaviour of the various insulation assemblies, an investigation was made to determine their ability to maintain thermal comfort and energy efficiency under various factors, including daily temperature fluctuations and climatic conditions. Consequently, a comparative analysis was conducted on the time lag parameter and the decrement factor for each insulation assembly.

The time lag refers to the duration that a heatwave requires to cross through an assembly from one surface to another. In another word, it represents the delay between the peak of a temperature on one surface and the corresponding temperature peak response on the opposing surface. A longer time lag indicates a slower heat transfer through a material.

Whereas, the decrement factor refers to the rate of attenuation in the amplitude of a heatwave as it propagates through an assembly. A higher decrement factor reflects a higher capacity of a material in dampening heat transfer.

The time lag  $\omega$  (h) and decrement factor  $f$  (-) can be obtained as shown in Eqs. (18) and (19) respectively (Ibrahim et al. 2014):

$$\omega = t_{int,max} - t_{ext,max} \quad (18)$$

$$f = \frac{T_{int, max} - T_{int, min}}{T_{ext, max} - T_{ext, min}} \quad (19)$$

Where  $t_{int,max}$  and  $t_{ext,max}$  represent the time when interior and exterior temperatures reach their respective peak values. Additionally,  $T_{int,max}$ ,  $T_{int,min}$ ,  $T_{ext,max}$  and  $T_{ext,min}$  represent the maximum and minimum temperatures attained by the internal and external surfaces, respectively.

### ***III.7 Bio-hygrothermal simulation***

Based on the hygrothermal simulation results for the studied insulation assemblies obtained from the WUFI®Plus software, mould growth risk assessment was conducted through bio-hygrothermal simulations. This assessment was carried out utilizing the WUFI®Bio software, which is widely used in literature for predicting the growth of mould and fungi on building materials (Koh et al. 2022) (Ho Ryu et al. 2015).

Based on the decisive parameters affecting mould growth, namely temperature, relative humidity and the substrate quality, the WUFI®Bio software generates the germination isopleth graphs. During each time step, with the changing ambient temperature and humidity, this software computes the transient water content within a spore of a material and compares it to the critical water content obtained from the moisture storage function of the material.

The WUFI®Bio software assumes that germination occurs and mycelium growth initiates when the water content in the model spore exceeds the critical water content. Once germination is established, the mycelium growth isopleth system is used to estimate the extent of growth. However, growth is assumed to be stopped when the water content in the spore falls below the critical water content. Nevertheless, it resumes growing instantly when the critical water content is exceeded again.

It is to be noted that the WUFI®Bio software does not incorporate biogenic factors, pH value, surface quality and several other influential factors that can potentially hinder the process of germination and growth. Thus, the simulation results tend to be conservative, indicating a higher risk of mould growth compared to real conditions.

In this study, the S/BP and hemp concrete materials used are treated as surfaces within constructions, without direct contact to indoor air. Moreover, they are presumed to belong to substrate class I, denoting bio-utilizable substrates. Risk levels of each assembly were assessed based on the mould growth rate MGR (mm/year) measured on a yearly basis, mould index MI (-) and signal light.

#### IV. Results and discussions

##### IV.1 Experimental findings

##### IV.1.1 Water vapour permeability

The results of water vapour permeability and water vapour resistance factor for the S/BP composite under elevated humidity conditions, determined using the “wet cup” method are presented in table 5.

**Table 5**

Water vapour permeability  $\delta$  (kg/m.s.Pa) and water vapour resistance factor  $\mu$  comparison of S/BP composite for lower and higher humidities conditions.

$\delta$ value x E-11(kg/m.s.Pa)				$\mu$ Value (-)			
"dry cup"	Reference	"wet cup"	Reference	"dry cup"	Reference	"wet cup"	Reference
$6.98 \times 10^{-12} \pm 0,25 \times 10^{-12}$	Karaky (2018)	$5.82 \times 10^{-11} \pm 4.8 \times 10^{-12}$	This study	$28,67 \pm 1.02$	Karaky (2018)	$3.45 \pm 0.3$	This study

It is evident that the water vapour resistance factor  $\mu$ , as determined through the “dry cup” method for the S/BP composite, exhibits a higher value compared to its corresponding value obtained by the “wet cup” test method for the same composite.

Moreover, the obtained water vapour resistance factor  $\mu = 3.45$  at higher humidities conditions for S/BP composite is slightly higher than the water vapour resistance at higher humidities conditions of other biomaterials suitable for building insulation listed in table 6. This is credited to the small size of the beet pulps (2–4 mm) and to the high mass ratio of starch/BP equal to 40%, which provides a more homogenous and less porous composite than the others. Finally, the analysed S/BP composite exhibited a relatively low water vapour resistance factor  $\mu$ , rendering it well-suited for humidity moderation.

**Table 6**

Water vapour resistance factor  $\mu$  at higher humidities conditions for S/BP composite and other biomaterials suitable for thermal insulation.

Material		$\mu$ Value (–) "wet cup" test	References
S/BP		$3.45 \pm 0.3$	This study
Hemp concrete		1.43	Seng & coll. (2019)
Various Hemp bio-insulation materials	30% Hemp fibre, 60% wood fibre, 10% polyester	1.85	Latif & coll. (2014)
	85% Hemp fibres, 10–12% bicomponent fibres and 3–5% soda	1.28	
	70% Hemp fibres, 15% hemp shive, 8% ammonium phosphate, 7% polyolefin fibres	1.11	
	95% Hemp fibres and 5% combination recycled adhesive binder	1.1	
	35% Hemp fibre, 35% recovered waste cotton fibre, 15% bi-component polyester fibre and 15% fire retardant	0.51	
Wood fibreboard		$1.12 \pm 0.28$	Jerman & coll. (2019)
flax fibres		$1.03 \pm 0.28$	
hemp fibres		$1.46 \pm 0.62$	
jute fibres		$1.23 \pm 0.31$	
sheep wool		$1.62 \pm 0.62$	

#### IV.1.2 Capillary absorption coefficient

For each brick, the mass of water absorbed by per face area  $\Delta m_t$  ( $\text{Kg}/\text{m}^2$ ) was plotted as a function of the square root of time as shown in Fig. 7.

It can be observed that the curves are not linear but rather exhibit various non-linear forms and thus were considered as type **B** according to European standard NF EN ISO 15148:2003. Consequently, the capillary absorption coefficient ( $\text{Kg}/\text{m}^2 \cdot \text{S}^{0.5}$ ) through partial immersion was determined based on the water absorbed after 24 hours, as shown in Eq. (20) :

$$A_{w, 24} = \frac{\Delta m_t f}{\sqrt{86400}} \quad (20)$$



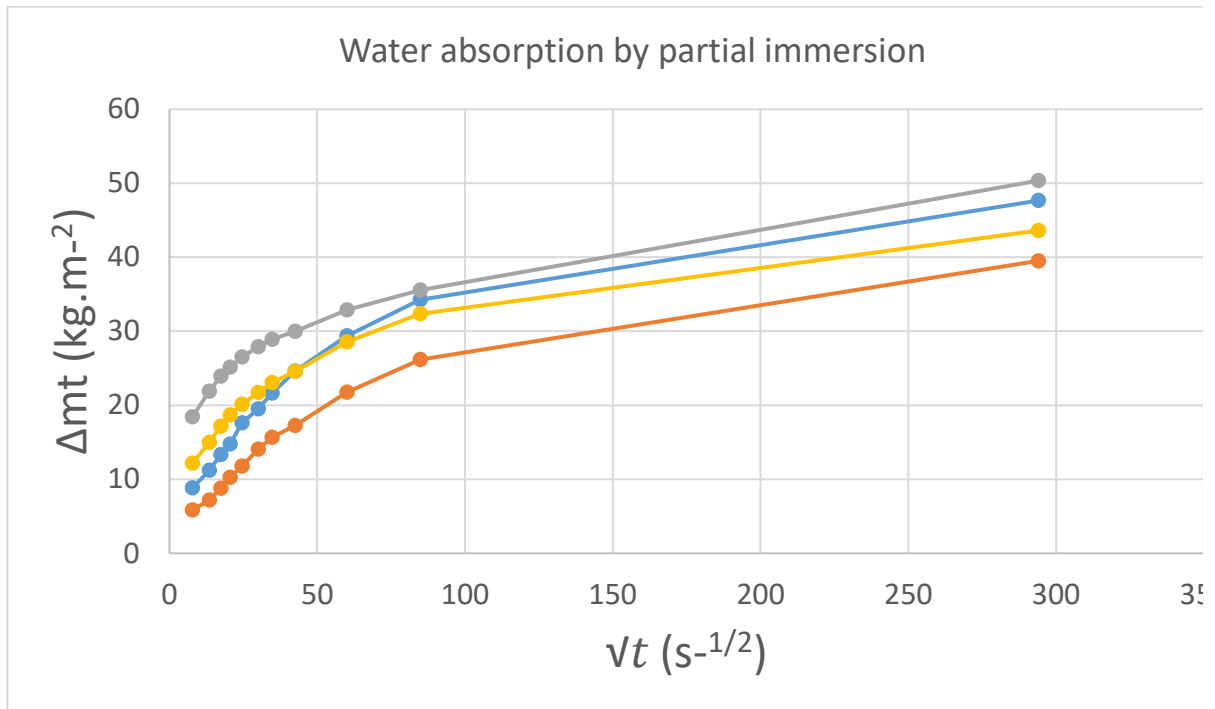


Figure 7: Measurements of the water absorption coefficient by partial immersion of the S/BP bricks

It was observed that prolonged exposure to liquid water has led to alterations in the surface structure of the S/BP insulation brick is in contact with water, with a noticeable increase in density near the surface. Consequently, the S/BP composite was deemed unsuitable for external insulation purposes. The results obtained for the capillary absorption coefficient by partial immersion  $A_w$  of the S/BP composite were found equal to  $0.154 \pm 0.016 \text{ Kg/m}^2 \cdot \text{S}^{0.5}$ . This value, as presented in table 7, was observed to be greater than  $A_w$  values for hemp concrete (Seng et al. 2019) and other various hemp-bio insulations materials (Latif et al. 2014), while being lower than  $A_w$  values for Wood fibreboard, flax fibres, jute fibres (Jerman et al. 2019).

**Table 7**

Water absorption coefficient by partial immersion  $A_w$  for S/BP composite and other biomaterials suitable for thermal insulation.

Material		$A_w$	References
S/BP		$0.154 \pm 0.016$	This study
hemp concrete		$0.14 \pm 0.01$	Seng & coll. (2019)
Various Hemp bio-	30% Hemp fibre, 60% wood fibre, 10% polyester 17	0.041	Latif & coll. (2014)
	85% Hemp fibres, 10–12% bicomponent fibres and 3–5% soda	0.034	

insulation materials	70% Hemp fibres, 15% hemp shive, 8% ammonium phosphate, 7% polyolefin fibres	0.033	
	95% Hemp fibres and 5% combination recycled adhesive binder	0.029	
	35% Hemp fibre, 35% recovered waste cotton fibre, 15% bi-component polyester fibre and 15% fire retardant	0.031	
Wood fibreboard		0.18 ± 0.03	Jerman & coll. (2019)
flax fibres		0.35 ± 0.08	
jute fibres		0.52 ± 0.1	
sheep wool		0.14 ± 0.03	

#### **IV.1.3 Moisture content at free saturation**

Owing to the important hydrophilic character of Beet Pulps by having their pores easily accessible and quickly filled with water leading to material swelling (Monreal et al. 2011), test specimens were weighed after 24 and 96 hours.

A rapid increase in the mass of the S/BP bricks was observed after first hours of immersion in water while a relatively minor change was observed after 24 hours. Therefore, the test was stopped after 96 hours of immersion in order to avoid structural damages on the tested bricks.

The density of water was assumed to be 1000 kg/m<sup>3</sup> and the obtained results for W<sub>lt</sub> and W<sub>f</sub> for S/BP bio composites bricks were respectively equal to 64.16 ± 3.74 volume % and 641.59 ± 37.43 Kg/m<sup>3</sup>.

#### **IV.1.4 Thermal conductivity**

The thermal conductivity tests carried out on the S/BP bio-composite having a mass ratio equal to 0.4 at an ambient temperature of 20 °C and a relative humidity of 60 % yielded to a thermal conductivity equal to 0.108 ± 0.0193 W/m.K . This value exceeded the thermal conductivity observed for the same material at an ambient temperature of 20 °C and a relative humidity of 10 % which was determined to be equal to 0.0757 W/(m·K) (Karaky et al. 2019).

Therefore, the increase in relative humidities levels lead to a reduction in the insulation effectiveness of the S/BP bio-composite which can be attributed to its hydrophilic nature. As relative humidities levels increase, the material's capacity to absorb water increases. The

absorbed water molecules displace the air within the pores, which will lead to a more efficient heat conduction inside the material as water exhibits superior thermal conductivities compared to air. Moreover, the presence of these water molecules can also exert an influence on the material fibres properties as they may experience swelling or even changes in their physical structure, furtherly contributing to the evolving thermal characteristics of the studied S/BP composite.

## **IV.2 Numerical simulation**

### **IV.2.1 Hygrothermal simulation**

#### **IV.2.1.1 Energy performance**

An energy performance analysis detailing the required cooling and heating loads was conducted on each insulation assembly. The findings were subsequently compared with the energy consumption of the baseline configuration under Nancy's and Marseille's Climates. The outcomes of these studies are outlined in Table 8.

**Table 8**

Energy consumption analysis of various insulation assemblies with S/BP or HC under Nancy's and Marseille's climates.

Conf.	Case	Under Nancy's climate				Under Marseille's climate			
		Heating Load (kWh)	Cooling Load (kWh)	Annual Total Load (kWh)	Reduction in total energy consumption (%)	Heating Load (kWh)	Cooling Load (kWh)	Annual Total Load (kWh)	Reduction in total energy consumption (%)
Primary	(0)	3104	334	3437	-	981	1421	2402	-
Insulation material based on Hemp concrete	(a)	2262	398	2660	22.6%	614	1284	1898	21.0%
	(b)	1845	455	2301	33.1%	430	1384	1814	24.5%
	(c)	1796	464	2260	34.3%	409	1398	1807	24.8%
	(d)	1765	470	2236	35.0%	397	1408	1804	24.9%
Insulation material based on Starch/Beet-pulp	(a)	2152	413	2566	25.4%	556	1308	1864	22.4%
	(b)	1730	472	2201	36.0%	372	1406	1778	26.0%
	(c)	1678	482	2160	37.2%	351	1427	1777	26.0%
	(d)	1663	485	2148	37.5%	345	1432	1777	26.0%

Table 8 shows that for Nancy's climate, heating demand exceeds the cooling one whereas for Marseille it is the opposite. This was expected given that Nancy's climate having a mean temperature equal to 9.16 °C is colder than Marseille's climate with a mean temperature equal to 15.42 °C, as shown in Fig. 3 and Fig. 5 respectively. The total annual energy demand for the primary scenario (case 0) within Nancy's climatic conditions was determined to be 3437 kWh, 43.1% higher compared to the corresponding total annual energy demand under Marseille's climatic conditions.

The incorporation of bio-insulation materials in accordance with case (a), resulted in a slight increase in annual cooling demand but a more substantial reduction in heating demand, leading to a decrease in total required annual energy consumption to 2660 kWh and 1898 kWh for HC and to 2566 kWh and 1864 kWh for S/BP under Nancy's and Marseille's climates, respectively. Hence, a reduction in total energy consumption relative to case (0) was achieved equal to 22.6% and 21% for HC and 25.4% and 22.4% under the two studied climates, respectively. A further reduction in total energy consumption was achieved when increasing the thickness of bio-insulations materials from 10 cm to 20 cm in accordance with case (b) where it reached 2301 kWh and 1814 kWh for HC and 2201 kWh and 1778 kWh for S/BP under Nancy's and Marseille's climates, respectively.

The additional insertion of air layer in accordance with case (c), resulted in a further decrease in the total required annual energy consumption yielding 2260 kWh and 1807 kWh for HC and 2160 kWh and 1777 kWh for S/BP under Nancy's and Marseille's climates, respectively.

For case (d), a marginal decrease in energy consumption of 0.7% for HC and 0.3% for S/BP was observed Under Nancy's climate, in comparison to case (c). Conversely, there was no observed improvement in energy consumption under Marseille's climate.

Furthermore, the S/BP bio-composite exhibited a superior effectiveness compared to HC for thermal insulation use under the studied climatic conditions. This outcome was predicted, given that the thermal conductivity of HC is greater than that of S/BP.

#### ***IV.2.1.2 Dryness rate***

The initial RH was set at 80% for all various components comprising the insulation assemblies.

The total water content for each assembly was documented initially and subsequently after each year for a total duration of 4 years. The outcomes of these studies are outlined in Table 9. As a result, the dryness rate for each assembly was calculated and subsequently depicted graphically, as illustrated in Fig. 8.

**Table 9**

Total water content analysis of insulation assemblies with S/BP or HC under Nancy's and Marseille's climates.

Config.	Case	Under Nancy's climate					Under Marseille's climate				
		TWC i	TWC 1	TWC 2	TWC 3	TWC f	TWC i	TWC 1	TWC 2	TWC 3	TWC 4
Insulation material based on Hemp concrete	(a)	10.02	10.83	10.95	11.00	10.98	10.02	12.85	13.32	13.42	13.44
	(b)	12.05	13.14	13.31	13.38	13.38	12.05	15.24	15.93	16.11	16.15
	(c)	12.05	13.16	13.33	13.40	13.39	12.05	15.24	15.92	16.10	16.14
	(d)	12.05	13.19	13.37	13.44	13.43	12.05	15.26	15.95	16.13	16.17
Insulation material based on Starch/Beet-pulp	(a)	13.31	13.82	13.78	13.79	13.77	13.31	16.08	16.64	16.79	16.82
	(b)	18.64	19.29	19.08	19.00	18.93	18.64	21.60	22.32	22.58	22.66
	(c)	18.64	19.26	18.99	18.87	18.78	18.64	21.57	22.22	22.44	22.50
	(d)	18.64	19.27	18.98	18.85	18.77	18.64	21.57	22.21	22.42	22.49

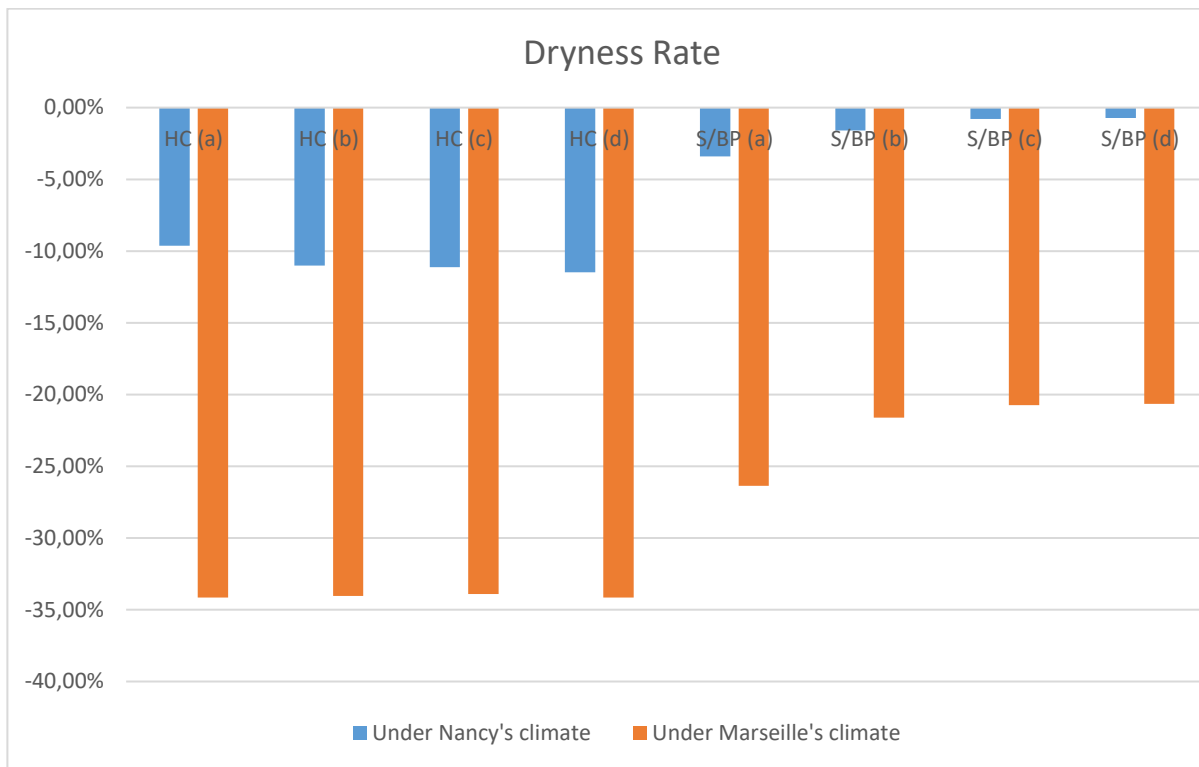


**Figure 8: Dryness rate of insulation assemblies with S/BP or HC under Nancy's and Marseille's climates**

Under Nancy's climate, the TWC of Insulation assemblies based on HC initially increased, eventually reaching a quasi-steady state after 4 years for the four cases. In contrast, TWC of insulation assemblies based on S/BP exhibited an initial increase, followed by attainment of a quasi-steady-state after 4 years for only case (a). Whereas, the TWC for the remaining 3 cases began to gradually decrease progressively after the first year, reflecting the superior abilities of these assemblies to dry out and thereby exchanging moisture with their surroundings without accumulating it internally. These findings are consistent with the computed results regarding the annual mean inner and outer moisture flux entering and leaving the studied insulation assemblies, as shown in Fig. 9.

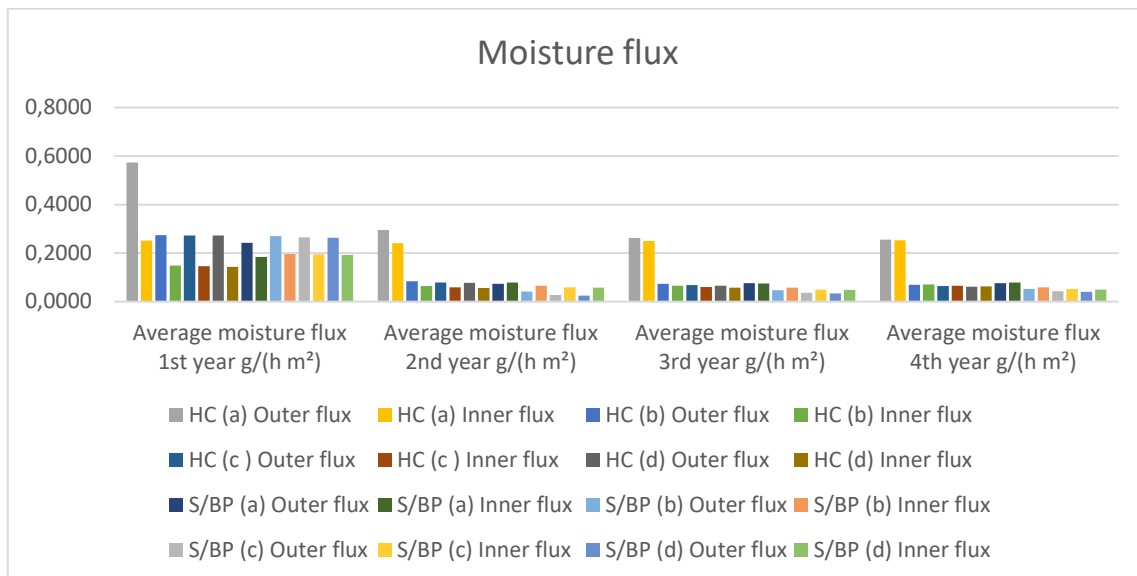


**Figure 9: Annual mean inner and outer moisture flux throughout insulation assemblies with S/BP or HC under Nancy's climate**

Conversely, the TWC is about 20% higher for each case when considering Marseille's climate in comparison to that of Nancy. The TWC showed a continuous, gradual increase over the 4 years, reflecting reduced abilities of these assemblies to dry out under Marseille's climate and resulting in the accumulation of moisture internally. This in turn, heightens the risk of bio-deterioration mould, and decay damages within these structures.

For Nancy conditions, insulation assemblies based on S/BP demonstrated superior DR in comparison to Marseille's climate. For cases (a), (b), (c) and (d), the DR was equal to -3.4 %, -1.59 %, -0.79 %, -0.72 %, respectively under Nancy's climate while they were notably lower at -26.37 %, -21.6 %, -20.74 %, -20.65 % under Marseille's climate. This can be attributed to the higher levels of absolute humidity in Marseille's climate compared to those in Nancy. Consequently, higher relative humidity levels will occur in the indoors, resulting in an increase in the TWC within the assembly and a subsequent decrease in the DR.

Whereas, the Insulation assemblies based on HC exhibited DR values of -9.63 %, -11.01 %, -11.12 %, -11.48 % for the same cases respectively under Nancy's climate, and substantially lower values of -34.15 %, -34.04 %, -33.90 %, -34.15 % under Marseille's climate.

It can be deduced that Insulation assemblies based on S/BP exhibited superior dryness rate compared to HC under both Nancy's and Marseille's climates. This can be attributed to the

higher thermal insulation of S/BP, which helps raise the average temperature within the wall and therefore delays saturation and enhances dryness.

Finally, an optimal DR was observed under the Nancy’s climate for case (d) for insulation assembly made of S/BP and for case (a) for insulation assembly made of HC.

**IV.2.1.3 Condensation risk**

All studied cases exhibited a complete absence of condensation risk on the internal surfaces of diverse assemblies. However, internal condensation risks manifested within the studied assemblies under both Nancy’s and Marseille’s climate. These risks were assessed by calculating the proportion of time during which criteria A, B or C (ASHRAE, 2008) were not satisfied. The results of these studies are illustrated in Fig. 10.

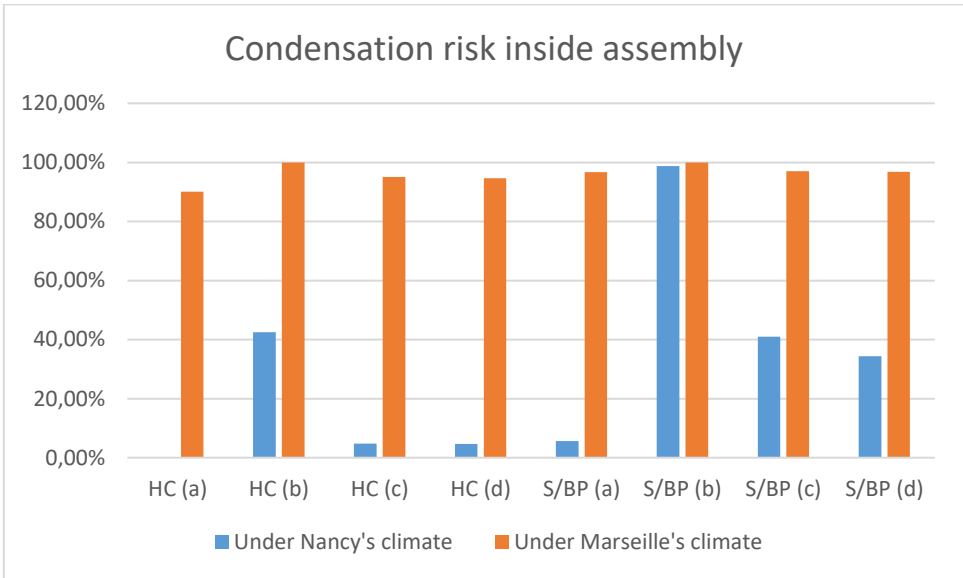


**Figure 10: Condensation risk inside insulation assemblies with S/BP or HC under Nancy’s and Marseille’s climates**

Increasing insulation thickness from 10 cm to 20 cm resulted in a CR increase for HC from 0% to 42.46% under Nancy’s climate and from 90.05% to 100% under Marseille’s climate. Incorporating 2 cm and 4 cm air layers in the assembly led to a more effective decrease in CR, reducing it to 4.79 % and 4.63% respectively under Nancy’s climate. However, a minor decrease in CR to only 95.03% and 94.66% under Marseille’s climate was observed after adding the 2 cm and 4 cm air layers, respectively.



As for S/BP, increasing insulation thickness from 10 cm to 20 cm increased CR from 5.61% up to 98.78% under Nancy's climate and from 96.67% to 100% under Marseille's climates. Incorporating 2 cm and 4 cm air layer in these assemblies led to a minor decrease in CR to 95.03% and 94.66% under Nancy's climate and to 96.98% and 96.79% under Marseille's climate, respectively.

It can be deduced that Insulation assemblies based on S/BP exhibited higher CR within the wall compared to HC for the same assembly configuration under both analysed climatic conditions. This can be attributed to the elevated water vapour permeability of HC in contrast to S/BP.

Furthermore, it was noted that a higher CR was consistently observed under Marseille's climate for the same studied configuration due to the increased frequency in days with higher absolute humidities compared to Nancy's climate. Lastly, the optimal CR was observed for case (a) for both insulation assemblies based on S/BP and HC under Nancy's climate.

#### ***IV.2.1.4 Dynamic thermal behavior***

In order to optimize the dynamic thermal behaviour is essential to achieve a higher time lag and a lower decrement factor. This can be realized through increasing wall thickness and reducing its overall thermal diffusivity, which involves minimizing the thermal diffusivities of the individual layers constituting the wall. For this purpose, the time lag and decrement factor for each assembly were documented. The outcomes of these studies are outlined in Table 10.

**Table 10**

Time lag and decrement factor of insulation assemblies with S/BP or HC under Nancy's and Marseille's climates.

Conf.	Case	Under Nancy's climate		Under Marseille's climate	
		Time lag $\omega$ (h)	Decrement factor f (-)	Time lag $\omega$ (h)	Decrement factor f (-)
Primary	0	7	0.1273	10	0.0932
Insulation material based on	(a)	6	0.0809	7	0.0432
	(b)	6	0.0831	7	0.0415
	(c)	6	0.0825	7	0.0411

<b>Hemp concrete</b>	(d)	6	0.0825	7	0.0411
<b>Insulation material based on Starch/Beet-pulp</b>	(a)	6	0.0825	6	0.0410
	(b)	6	0.0896	6	0.0470
	(c)	6	0.0894	6	0.0459
	(d)	6	0.0825	6	0.0458

Insulation materials based on HC exhibited a time lag of around 6 hours under Nancy's climate and around 7 hours under Marseille's climate. However, Insulation materials based on S/BP exhibited a time lag of around 6 hours under both Nancy's and Marseille's climates.

As for the decrement factor, the increase of insulation thickness from 10 cm to 20 cm under Nancy's climate resulted in its increase from 0.0809 to 0.0831 and from 0.0825 to 0.0896 for insulation assemblies based on HC and S/BP respectively. Conversely, a reduction in the decrement factor was observed subsequent to the incorporation of air layers as it reached 0.0825 for Insulation materials based on HC and S/BP for an air layer of 4 cm. This is expected, as the incorporation of an air layers induces an increase in the thermal resistance of the assembly.

However, within the climatic conditions of Marseille, a substantial reduction in decrement factor was noted when compared to Nancy's climate. This reduction averaged 49.2% and 47.8% for insulation assemblies with HC and S/BP respectively. This is attributed to the elevated total water content within the assembly in Marseille's climate compared to Nancy's climate. This increase in TWC augments the thermal mass of the assembly, enabling the storage of a greater amount of thermal energy and exhibiting therefore a damping effect on the decrement factor.

It is notable that the acquired values of time lag and decrement factor are significantly impacted by the control of indoor air temperature through the imposed air conditioning system.

Eventually, Insulation assemblies based on S/BP and HC displayed superior dynamic thermal behaviour under Marseille's climates. Notably, an optimal time lag and decrement factor was

observed for case (d) for insulation assembly with HC and for case (a) for insulation assembly with S/BP.

**IV.2.2 Bio-hygrothermal simulation**

As soon as the computed water content in the spore exceeds the critical water content, it is presumed that spore germination occurs and initiates mycelium grows. This growth is assumed to stop when the water content within the spore drops below the critical water content.

The fluctuations in water content within the spore with time, the critical water content for mycelium germination and the mould growth rate for each insulation assembly based on HC over a duration of 4 years are illustrated in Fig. 11 and Fig. 12 under Nancy’s and Marseille’s climates, respectively. Conversely, the aforementioned studies conducted on insulation assemblies based on S/BP are illustrated in Fig. 13 and Fig. 14 under the respective studied climates.

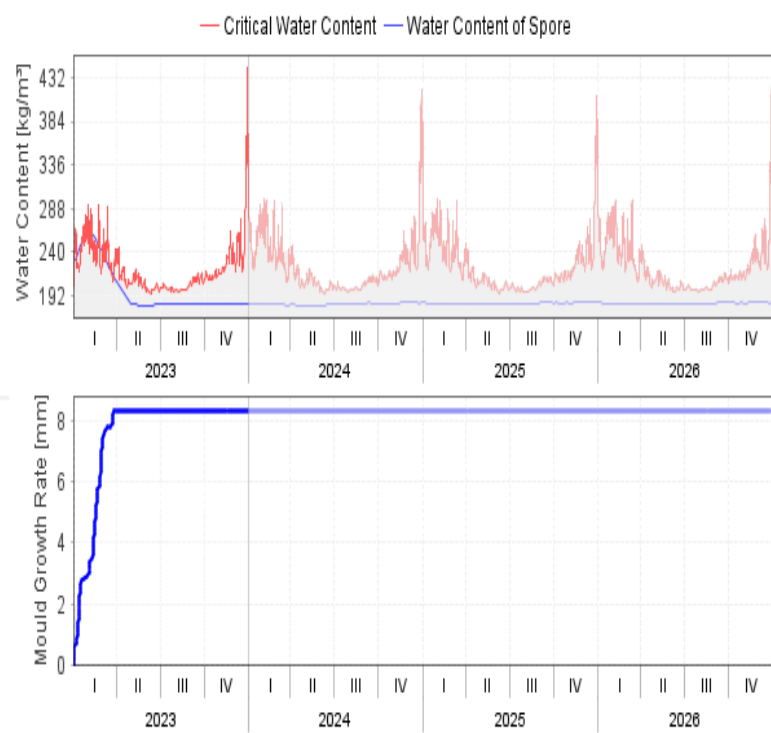
Furthermore, the signal light provides a comprehensive evaluation of the potential mould growth risk and the severity of the infestation, if present. For an occupant exposition class, which in this study pertains to Surfaces inside constructions without direct contact to indoor air, if the mould growth rate (MG) falls within the range of 176 to 239 mm/year and the mould index (MI) is between 2 and 3, a yellow signal light is displayed. This signifies the need for further criteria of investigations to assess safety and acceptability. Conversely, when the values fall below these thresholds, the signal light turns into green, denoting acceptability. However, exceeding these values causes the signal light to turn to green, indicating that the structure is at a significantly elevated risk of mould growth, rendering it unacceptable.

In this context, the MGR, MI and signal light of insulation assemblies based on S/BP or HC under Nancy's and Marseille's climates are outlined in table 11.

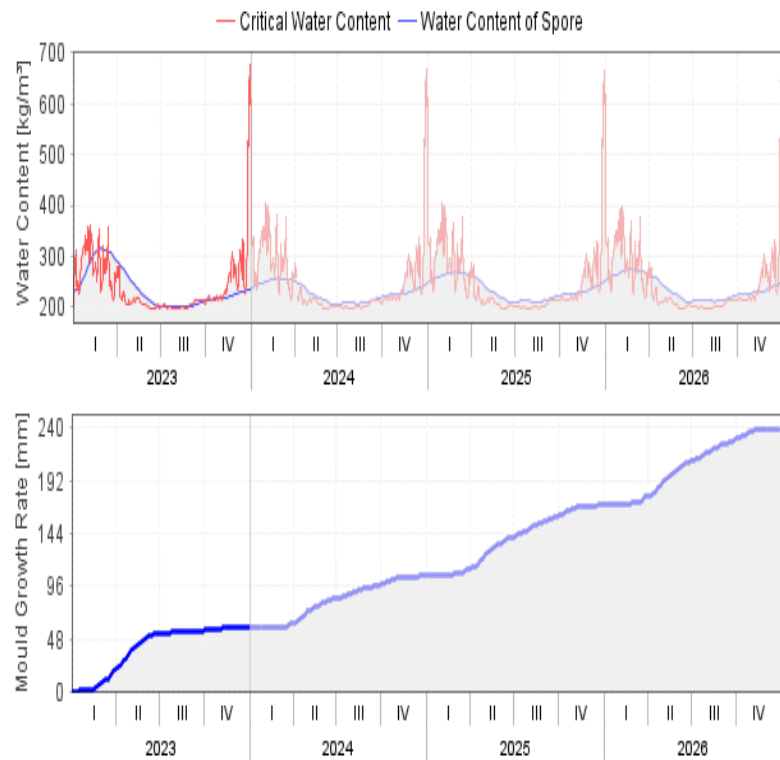
**Table 11**  
Mould growth rate, Mould index and signal light of insulation assemblies with S/BP or HC under Nancy's and Marseille's climates.

Conf.	Case	Under Nancy's climate	Under Marseille's climate
-------	------	-----------------------	---------------------------

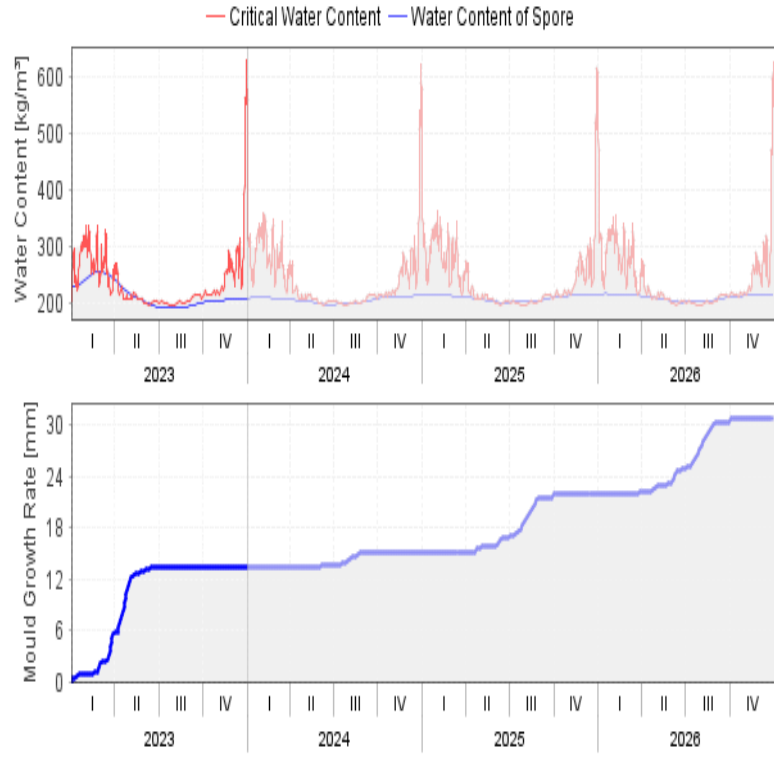
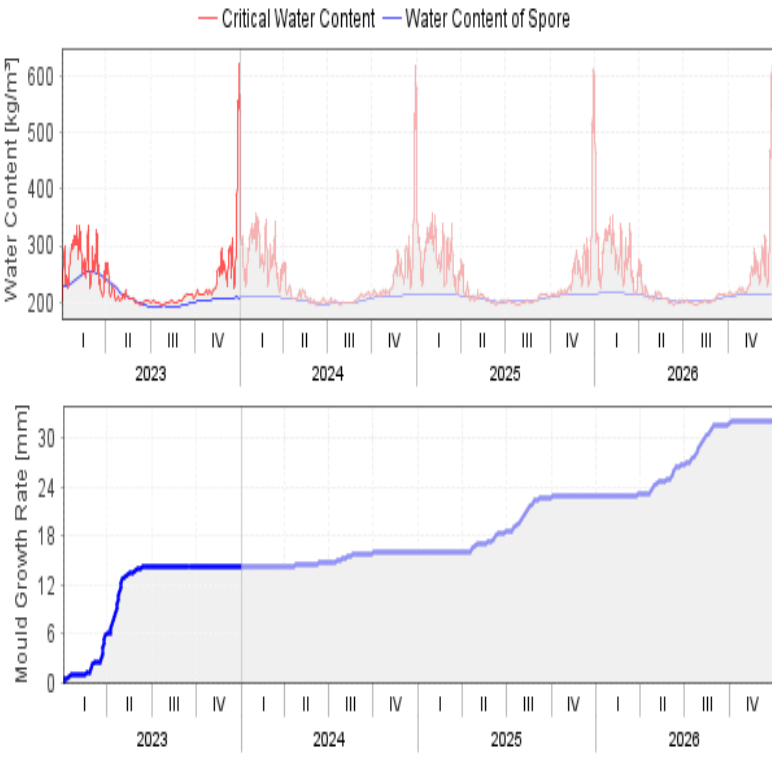
		MGR (mm/year)	MI (-)	Signal light	MGR (mm/year)	MI (-)	Signal light
<b>Insulation material based on Hemp concrete</b>	(a)	8.35	0.01	Green	149	1.45	Green
	(b)	57.8	0.16	Green	271	3.39	Red
	(c)	14.2	0.03	Green	198	2.4	Yellow
	(d)	13.4	0.02	Green	194	2.33	Yellow
<b>Insulation material based on Starch/Beet- pulp</b>	(a)	23.3	0.05	Green	207	2.54	Yellow
	(b)	140	1.25	Green	323	3.92	Red
	(c)	100	0.51	Green	264	3.31	Red
	(d)	95.9	0.45	Green	256	3.22	Red



HC – case (a)



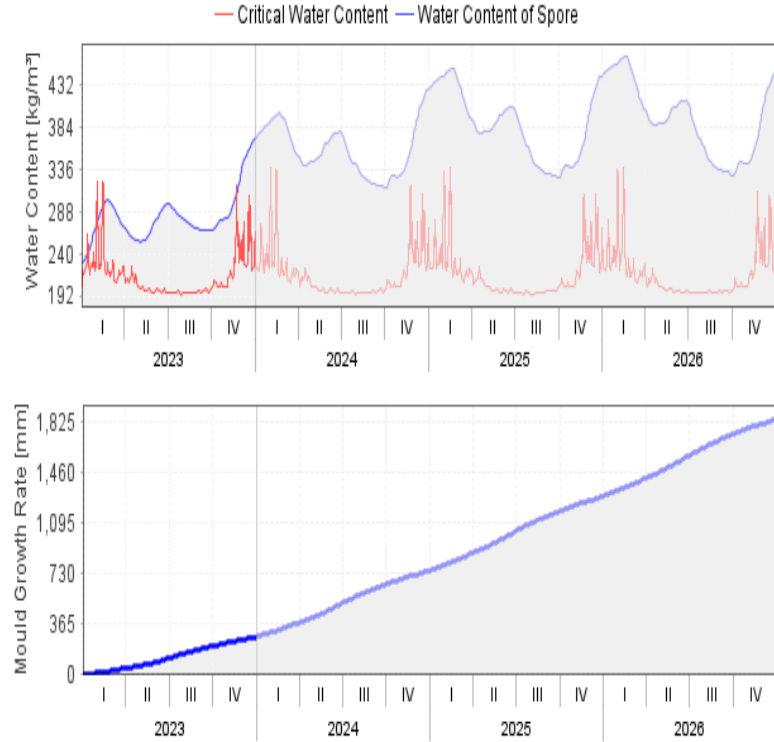
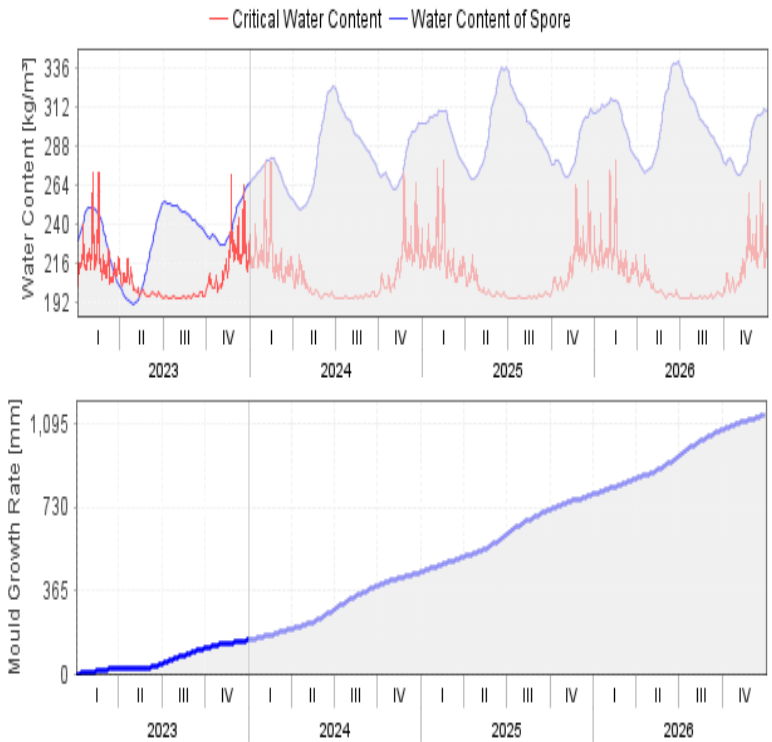
HC – case (b)



HC – case (c)

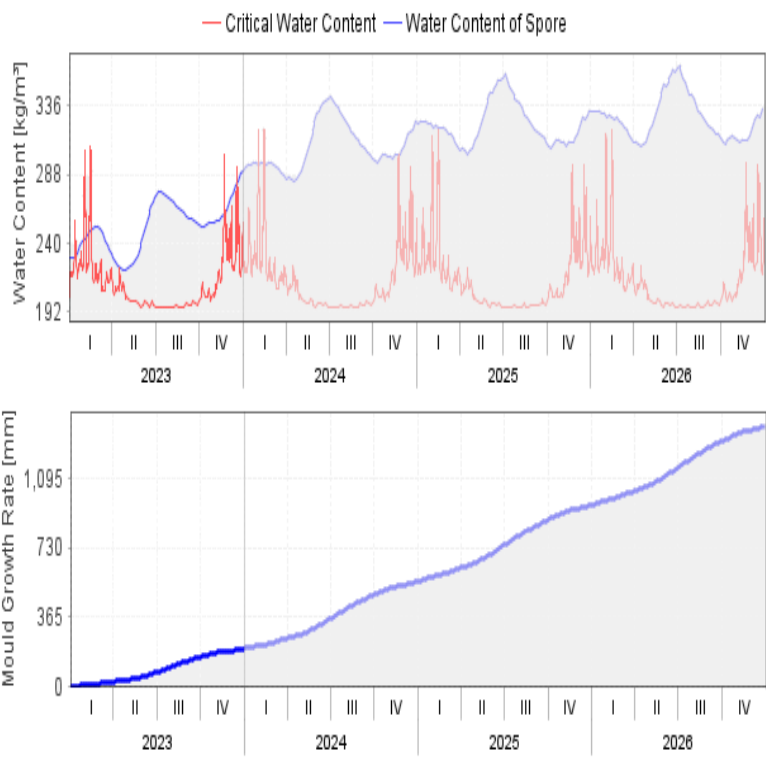
HC – case (d)

Figure 11: Water content and mould growth rate for various insulation assemblies with HC under Nancy's climate.

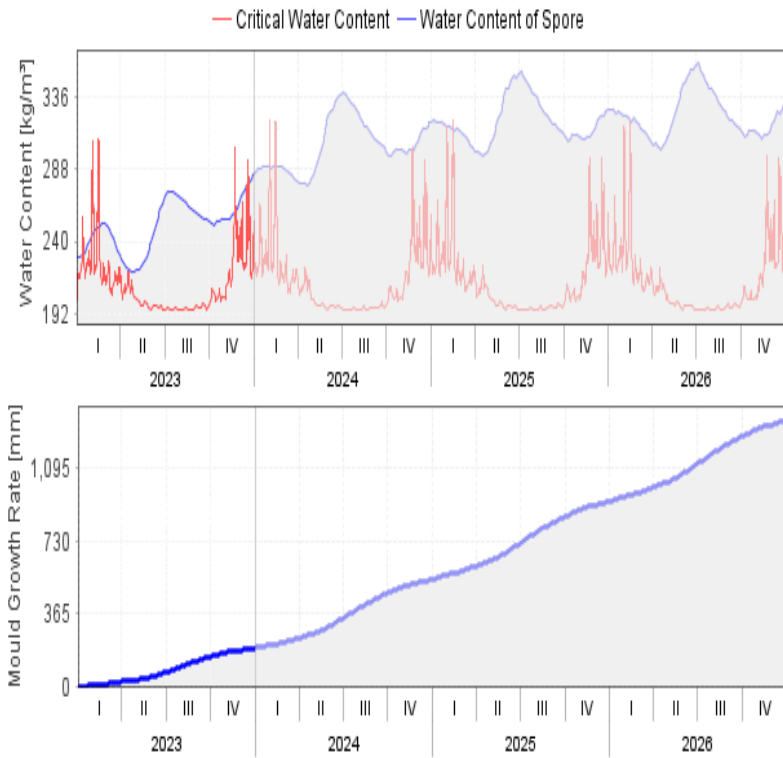


HC –case (a)

HC –case (b)

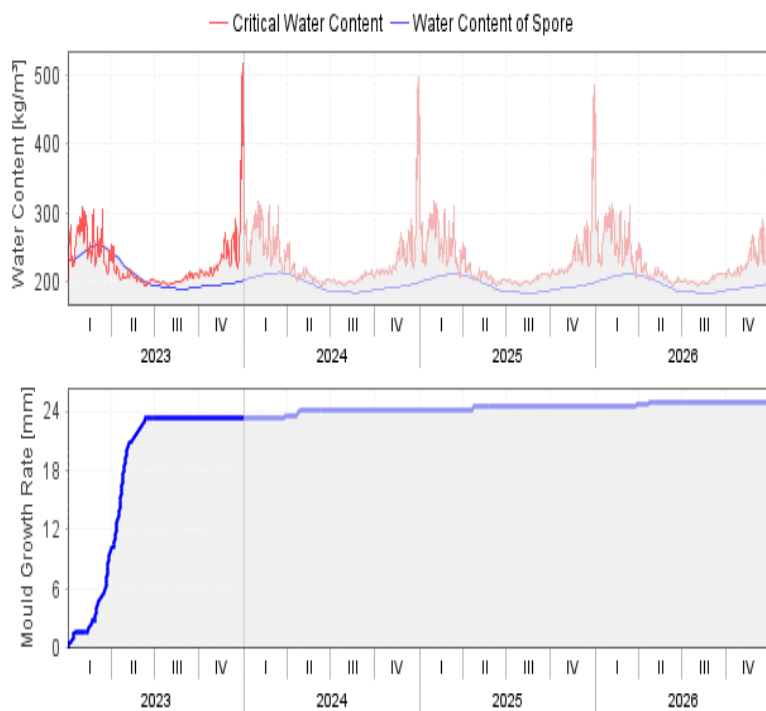


HC –case (c)

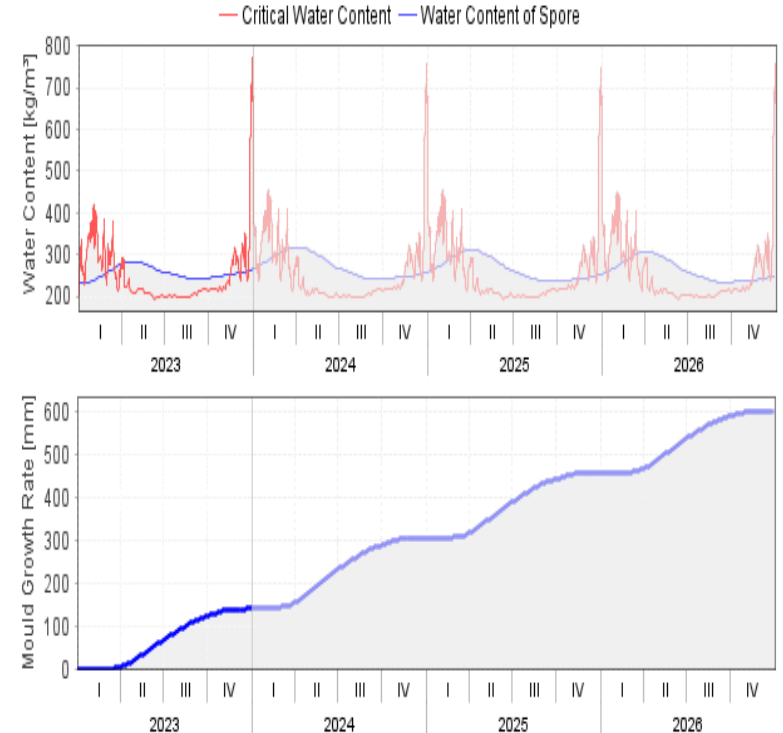


HC –case (d)

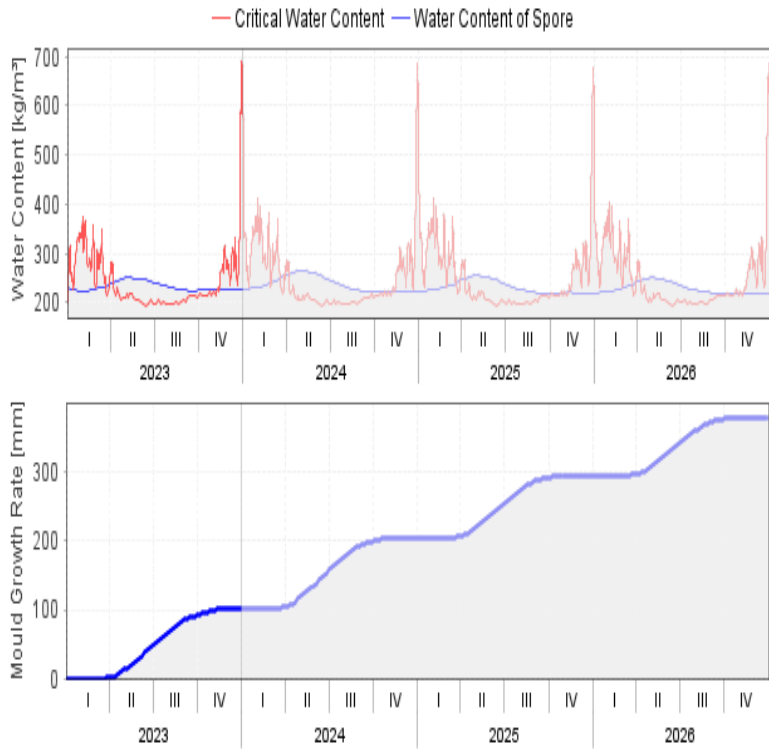
Figure 12: Water content and mould growth rate for various insulation assemblies with HC under Marseille’s climate.



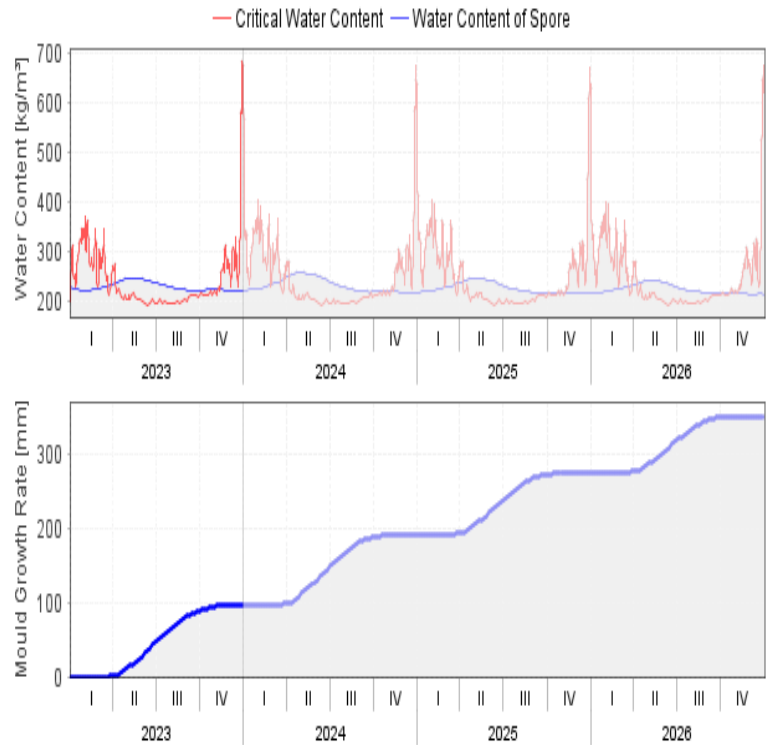
S/BP – case (a)



S/BP – case (b)

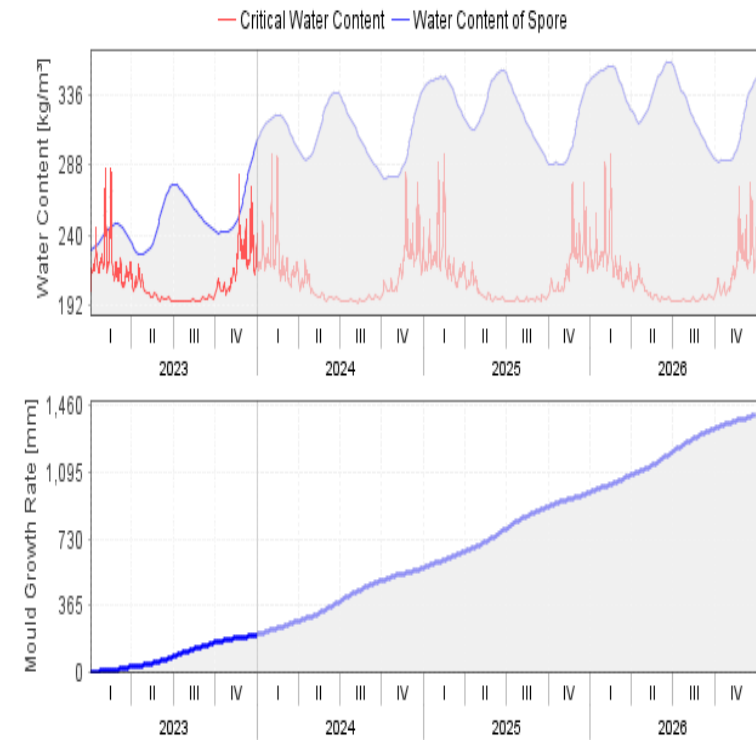


S/BP – case (c)

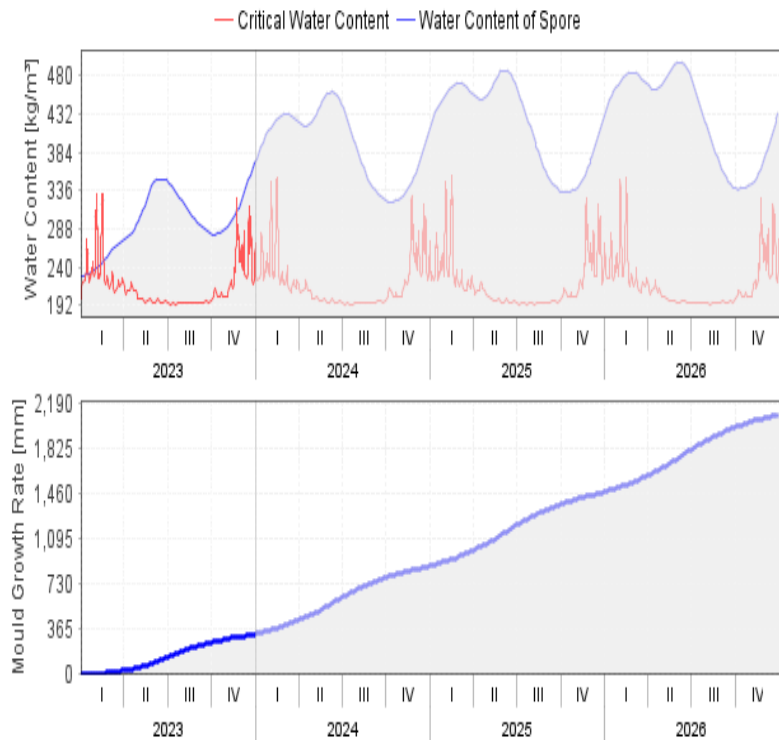


S/BP – case (d)

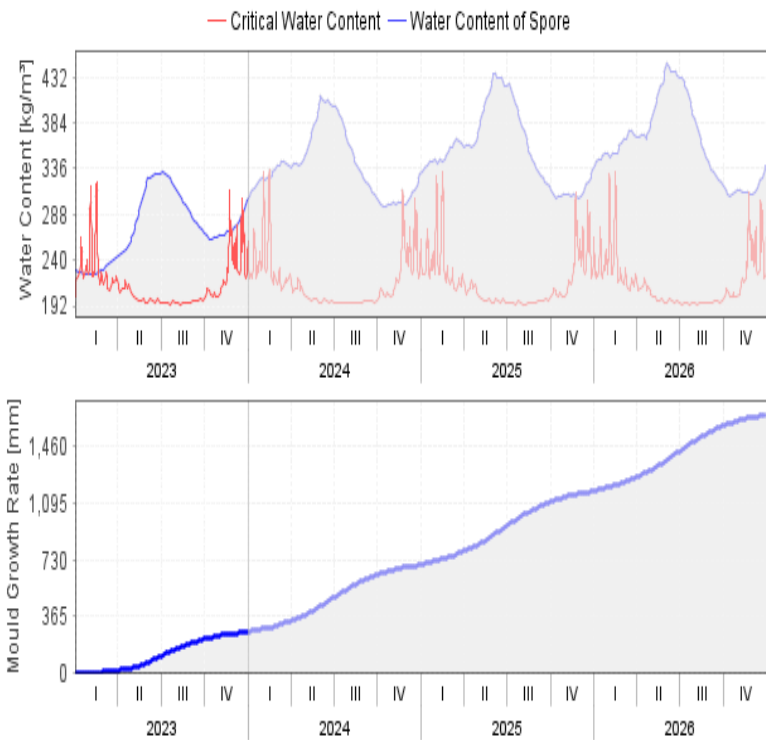
Figure 13: Water content and mould growth rate for various insulation assemblies with S/BP under Nancy's climate.



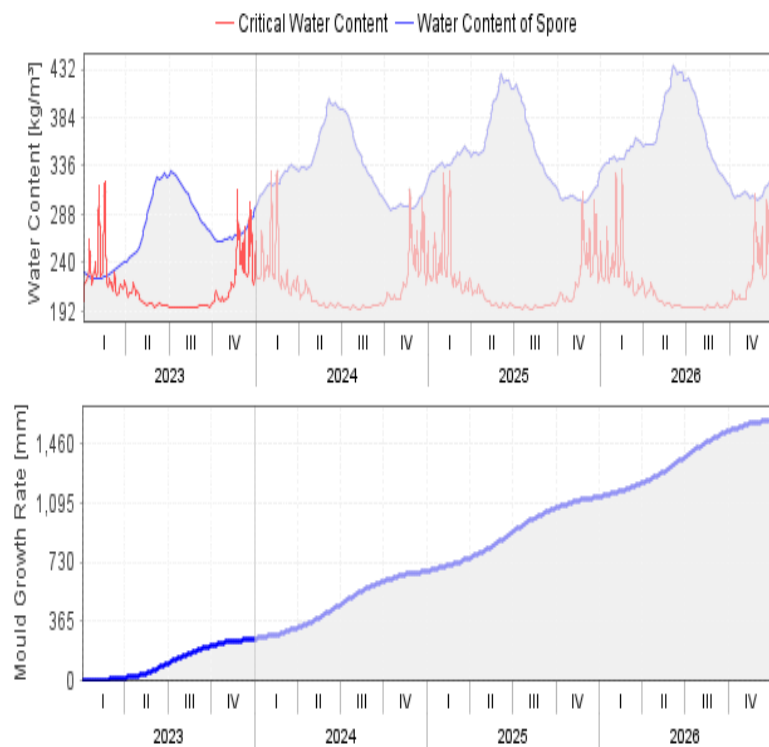
S/BP – case (a)



S/BP – case (b)



S/BP – case (c)



S/BP – case (d)

Figure 14: Water content and mould growth rate for various insulation assemblies with S/BP under Marseille’s climate

Under Nancy’s climate, all insulation assemblies exhibited a green signal light, affirming their acceptability. The increase in insulation thickness from 10 cm to 20 cm led to an increase in the MI from 0.01 to 0.16 for Insulation assemblies based on HC and from 0.05 to 1.25 for Insulation materials based on S/BP. This can be attributed to the increase in moisture absorption and to the prolonged periods of moisture retention due to the increase in bio-insulation material thickness.

The integration of air layer proved effective in reducing MI to 0.02 and 0.45 for Insulation assembly based on HC and S/BP respectively and for an air layer thickness of 4 cm. This can be attributed to the role of air layer as a barrier, effectively isolating the interior surfaces of the assembly from the exterior moisture sources, which helps in reducing the available moisture and maintaining a more stable environment.

Under Marseille’s climate, exclusively case (a) for insulation assemblies based on HC exhibited a green signal light with a MI value of 1.45. Whereas, case (b) displayed a red light with a maximum MI value of 3.39, while cases (c) and (d) displayed a yellow signal light. As for insulation assemblies based on S/BP, case (a) displayed a yellow signal light with a MI value of



2.54. Whereas remaining cases signalled a red light with a maximum MI value of 3.92 for case (b).

Hence, Insulation assemblies based on HC highlighted lower susceptibility to mould growth risk in comparison to insulation assemblies based on S/BP under both studied climatic conditions. This outcome was anticipated, given that HC has a higher water vapour permeability than S/BP, which prevents moisture accumulation and enables even moisture distribution and redistribution within the assembly, resulting in a reduced risk of mould growth. Furthermore, the risk of mould growth was found to be less pronounced under Nancy's climate, which can be attributed to the increased frequency in days with higher absolute humidities in Marseille compared to Nancy's climate.

## **V. Conclusion**

Initially, this study conducted an assessment on hygrothermal characteristics of an economically viable, bio-derived material made of starch and beet-pulp with a mass ratio equal to 40% for building insulation use. For this purpose, experimental studies were elaborated in order to determine the water vapour resistance factor under elevated humidities, capillary absorption coefficient, moisture content at free saturation and the thermal conductivity dependent on humidity. The results indicated favourable hygrothermal performance, rendering this material suitable for employment in internal building insulation. However, it was found unsuitable for external insulation use.

Afterwards, a comprehensive evaluation and comparison of the hygrothermal and bio-hygrothermal performances and behaviour of different multilayer insulation assemblies made of either Starch/Beet pulp or Hemp concrete were undertaken. This analysis entailed numerical simulations utilizing the WUFI® PLUS and WUFI®bio softwares, conducted within the climatic conditions of two distinct cities in France- Nancy and Marseille. The primary goal was to investigate the influence of insulation materials types, thickness, covering materials and the presence of an air layer on indoor hygrothermal comfort across varying outdoor weather conditions.

For each design, the overall energy performance, total water content, drying rate, condensation risk and mould growth were evaluated. The objective was to associate to each

specific climate the optimal assembly configuration from both hygric and thermal perspectives.

Results showed that insulation assemblies based on the:

- S/BP bio-composite exhibited a superior effectiveness compared to HC for potential energy savings in thermal insulation. This was particularly notable under Nancy's climate, with case (d) proving to be the most efficient configuration.
- S/BP bio-composite exhibited superior dryness rate compared to HC. This was particularly notable under Nancy's climate, with case (d) proving to be the most efficient configuration.
- S/BP bio-composite exhibited higher CR within the wall compared to HC. The optimal CR for S/BP was observed for case (a) under Nancy's climate.
- HC composite showcased superior dynamic thermal behaviour compared to S/BP, particularly under Marseille's climate. Notably, among all cases associated to S/BP, case (a) under Marseille's climate, proved to be the most efficient configuration when considering both the time lag and decrement factor perspectives.
- HC composite showcased lower susceptibility to mould growth risk compared to S/BP, particularly under Nancy's climate. Notably, among all cases associated to S/BP, case (a) under Nancy's climate, proved to be the most efficient configuration when considering both MGR and MI perspectives.

In conclusion, insulation assemblies based on S/BP demonstrated superior hygrothermal performance under Nancy's climate compared to that of Marseille. A more pronounced reduction in energy consumption, a decreased lower and more stable total water content variation, an improved dryness rate, a reduced condensation risk and a lower susceptibility to mould growth were observed under Nancy's climate for insulation assemblies based on S/BP. Conversely, the only notable improvement observed for these assemblies was a more favourable decrement factor under Marseille's climate. These results can be mainly attributed to the heightened frequency in days characterized with higher absolute humidities levels in Marseille compared to Nancy's climate.

## **VI. Acknowledgment**

The authors would like to thank Crystal Union Company for providing the beet-pulp necessary for the specimens manufacturing.

## VII. References

- European Commission. (2020, February 17). Energy efficiency in buildings. Retrieved May 24, 2023, from [https://commission.europa.eu/news/focus-energy-efficiency-buildings-2020-02-17\\_en](https://commission.europa.eu/news/focus-energy-efficiency-buildings-2020-02-17_en) .
- Omran, H., GhaffarianHoseini, A., GhaffarianHoseini, A., Raahemifar, K., & Tookey, J. (2016). Application of passive wall systems for improving the energy efficiency in buildings: A comprehensive review. *Renewable and Sustainable Energy Reviews*, 62, 1252–1269. <https://doi.org/10.1016/j.rser.2016.04.010>
- Kumar, D., Alam, M., Zou, P. X. W., Sanjayan, J. G., & Ahmed, R. (2020). Comparative analysis of building insulation material properties and performance. *Renewable and Sustainable Energy Reviews*, 131(March), 110038. <https://doi.org/10.1016/j.rser.2020.110038>
- Ascione, F., Bianco, N., Maria Mauro, G., & Napolitano, D. F. (2019). Building envelope design: Multi-objective optimization to minimize energy consumption, global cost and thermal discomfort. Application to different Italian climatic zones. *Energy*, 174, 359–374. <https://doi.org/10.1016/j.energy.2019.02.182>
- Electricité de France. (n.d.). Il était une fois les réglementations thermiques. Retrieved May 24, 2023, from <https://particulier.edf.fr/fr/accueil/economies-d-energie/construction-et-renovation/la-reglementation-thermique-2012/il-etait-une-fois-les-reglementations-thermiques>
- Ministère de la transition écologique. (2023, February 17.). Réglementation environnementale RE2020. Retrieved May 24 2023, from <https://www.ecologie.gouv.fr/reglementation-environnementale-re2020>
- Xue, Y., Fan, Y., Wang, Z., Gao, W., Sun, Z., & Ge, J. (2022). Facilitator of moisture accumulation in building envelopes and its influences on condensation and mould growth. *Energy and Buildings*, 277, 112528. <https://doi.org/10.1016/j.enbuild.2022.112528>
- Moon, H. J., Ryu, S. H., & Kim, J. T. (2014). The effect of moisture transportation on energy efficiency and IAQ in residential buildings. *Energy and Buildings*, 75, 439–446. <https://doi.org/10.1016/j.enbuild.2014.02.039>
- Menneer, T., Mueller, M., Sharpe, R. A., & Townley, S. (2022). Modelling mould growth in domestic environments using relative humidity and temperature. *Building and Environment*, 208(November 2021), 108583. <https://doi.org/10.1016/j.buildenv.2021.108583>
- Li, S., Zhang, X., Li, Y., Gao, W., Xiao, F., & Xu, Y. (2023). A comprehensive review of impact assessment of indoor thermal environment on work and cognitive performance

- Combined physiological measurements and machine learning. *Journal of Building Engineering*, 71(March), 106417. <https://doi.org/10.1016/j.jobe.2023.106417>
- K.A. Angelon-Gaetz, D.B. Richardson, S.W. Marshall, M.L. Hernandez (2016). Exploration of the effects of classroom humidity levels on teachers' respiratory symptoms *Int. Arch. Occup. Environ. Health*, 89 (2016), pp. 729-737, <https://doi.org/10.1007/s00420-016-1111-0>
- Rabbat, C., Awad, S., Villot, A., Rollet, D., & Andrès, Y. (2022). Sustainability of biomass-based insulation materials in buildings: Current status in France, end-of-life projections and energy recovery potentials. *Renewable and Sustainable Energy Reviews*, 156. <https://doi.org/10.1016/j.rser.2021.111962>
- Badouard, C., Bogard, F., Bliard, C., Lachi, M., Abbes, B., & Polidori, G. (2021). Development and characterization of viticulture by-products for building applications. *Construction and Building Materials*, 302(July). <https://doi.org/10.1016/j.conbuildmat.2021.124142>
- Jerman, M., Palomar, I., Kočí, V., & Černý, R. (2019). Thermal and hygric properties of biomaterials suitable for interior thermal insulation systems in historical and traditional buildings. *Building and Environment*, 154(March), 81–88. <https://doi.org/10.1016/j.buildenv.2019.03.020>
- Zhou, Y., Trabelsi, A., & El, M. (2023). Hygrothermal properties of insulation materials from rice straw and natural binders for buildings. *Construction and Building Materials*, 372(February), 130770. <https://doi.org/10.1016/j.conbuildmat.2023.130770>
- H.M. Künzle, Simultaneous Heat and Moisture Transport in Building Components –One- and Two-dimensional Calculation Using Simple Parameters (Ph.D. Thesis), Fraunhofer Institute of Building Physics, Stuttgart, Germany, 1995.
- Fraunhofer Institute for Building Physics IBP.WUFI Passes Benchmark Test of EN 15026: WUFI Complies with the General Requirements of Standard EN 15026 and Passes its Benchmark Test (2007)
- Deutsches Institut für Normung DIN EN 15026, Hygrothermal performance of building components and building elements – Assessment of moisture transfer by numerical simulation CEN, Brussels, Belgium (2007)
- Liuzzi, S., Rubino, C., & Stefanizzi, P. (2017). ScienceDirect. Use of clay and olive pruning waste for building materials with high hygrothermal performances Use of clay The and pruning waste for building materials with high hygrothermal performances Assessing the feasibility of using the heat temperature function for district heat demand forecast. *Energy Procedia*, 126, 234–241. <https://doi.org/10.1016/j.egypro.2017.08.145>
- Simon, S., Jiang, S., Hao, J. L., & Carli, J. N. De. (2021). Hygrothermal and mechanical performance of sustainable concrete: A simulated comparison of mix designs. *Journal of Building Engineering*, 34(November 2019), 101859. <https://doi.org/10.1016/j.jobe.2020.101859>

- Ho Ryu, S., Jun, H., & Tai, J. (2015). Evaluation of the influence of hygric properties of wallpapers on mould growth rates using hygrothermal simulation. *Energy & Buildings*, 98, 113–118. <https://doi.org/10.1016/j.enbuild.2014.09.058>
- Coelho, G. B. A., Silva, H. E., & Henriques, F. M. A. (2018). Calibrated hygrothermal simulation models for historical buildings. *Building and Environment*, 142(May), 439–450. <https://doi.org/10.1016/j.buildenv.2018.06.034>
- WUFI®. (2019, April 16). WUFI® Plus software. Retrieved May 25, 2023, from <https://wufi.de/en/software/wufi-plus/>
- Brambilla, A., & Gasparri, E. (2020). Hygrothermal behavior of emerging timber-based envelope technologies in Australia: A preliminary investigation on condensation and mould growth risk. *Journal of Cleaner Production*, 276, 124129. <https://doi.org/10.1016/j.jclepro.2020.124129>
- Tlajji, G., Pennec, F., Ouldboukhitine, S., Ibrahim, M., & Biwole, P. (2022). Hygrothermal performance of multilayer straw walls in different climates. *Construction and Building Materials*, 326(February), 126873. <https://doi.org/10.1016/j.conbuildmat.2022.126873>
- Karaky, Hamzé. (2018). “Élaboration et Caractérisation Physique et Hygrothermique d’un Agro-Matériau à Base de Pulpe de Betterave et d’amidon.” Thèse de l’Université de Reims-Champagne-Ardenne.
- Karaky, H., Id, C. M., Bliard, C., Moussa, T., Wakil, N. El, Lachi, M., & Polidori, G. (2018). Hygrothermal and Acoustical Performance of Starch-Beet Pulp Composites for Building Thermal Insulation. *Materials*, 2018, 11, 1622. <https://doi.org/10.3390/ma11091622>
- Karaky, H., Maalouf, C., Bliard, C., Gacoin, A., Lachi, M., El, N., & Polidori, G. (2019). Characterization of beet-pulp fibre reinforced potato starch biopolymer composites for building applications. *Construction and Building Materials*, 203, 711–721. <https://doi.org/10.1016/j.conbuildmat.2019.01.127>
- Costantine, G., Harb, E., Bliard, C., Maalouf, C., Kinab, E., Abbès, B., ... Polidori, G. (2020). Experimental characterization of starch / beet-pulp bricks for building applications: Drying kinetics and mechanical behavior. *Construction and Building Materials*, 264, 120270. <https://doi.org/10.1016/j.conbuildmat.2020.120270>
- Harb, E., Maalouf, C., Bliard, C., Tenpierik, M., Lachi, M., Bogard, F., & Polidori, G. (2023). Thermal performance of starch/beet-pulp composite bricks for building insulation at a wall scale. *Case Studies in Construction Materials*, 18(October 2022), e01851. <https://doi.org/10.1016/j.cscm.2023.e01851>
- Tenpierik, M. J., Lachi, M., Bliard, C., & Polidori, G. (2023). Experimental and numerical investigation of the thermal inertia of sugar-beet-pulp / starch based bricks enhanced with phase change materials. *Construction and Building Materials*, 383(March), 131367. <https://doi.org/10.1016/j.conbuildmat.2023.131367>

- Lee, J., Wi, S., Jin, S., Choi, J., & Kim, S. (2020). Prediction evaluating of moisture problems in light-weight wood structure: Perspectives on regional climates and building materials. *Building and Environment*, 168(July 2019), 106521. <https://doi.org/10.1016/j.buildenv.2019.106521>
- NF EN ISO 12572. (2016). Hygrothermal performance of building materials and products - Determination of water vapour transmission properties – Cup method. AFNOR 2016.
- NF EN ISO 15148. (2003). Hygrothermal performance of building materials and products – Determination of water absorption coefficient by partial immersion AFNOR 2003.
- NF EN ISO 16535. (2019). Thermal insulation products for building applications – Determination of long term water absorption by immersion. AFNOR 2019.
- Seng, B., Magniont, C., & Lorente, S. (2019a). Characterization of a precast hemp concrete block. Part II: Hygric properties. *Journal of Building Engineering*, 24(May 2018), 100579. <https://doi.org/10.1016/j.jobe.2018.09.007>
- Seng, B., Magniont, C., & Lorente, S. (2019b). Characterization of a precast hemp concrete. Part I: Physical and thermal properties. *Journal of Building Engineering*, 24(April 2018), 100540. <https://doi.org/10.1016/j.jobe.2018.07.016>
- Latif, E., Tucker, S., Anca, M., Chitral, D., & Newport, D. (2014). Hygric properties of hemp bio-insulations with differing compositions. *Construction and Building Materials*, 66, 702–711. <https://doi.org/10.1016/j.conbuildmat.2014.06.021>
- Monreal, P., Mboumba-Mamboundou, L. B., Dheilly, R. M., & Quéneudec, M. (2011). Effects of aggregate coating on the hygral properties of lignocellulosic composites. *Cement and Concrete Composites*, 33(2), 301–308. <https://doi.org/10.1016/j.cemconcomp.2010.10.017>
- Koh, C. H., Gauvin, F., Schollbach, K., & Brouwers, H. J. H. (2022). Investigation of material characteristics and hygrothermal performances of different bio-based insulation composites. *Construction and Building Materials*, 346(May), 128440. <https://doi.org/10.1016/j.conbuildmat.2022.128440>
- Feng, C., Lei, Y., Fang, J., Lu, B., Li, X., & Xue, X. (2022). Optimized radiative parameters of building roof surfaces for energy efficiency: Case studies in China. *Journal of Building Engineering*, 61(September), 105289. <https://doi.org/10.1016/j.jobe.2022.105289>
- ASHRAE, 2008. Standard 160-2008. Criteria for Moisture-Control Design Analysis in Buildings. *ASHRAE Transactions*, 114 PART 1, 167–171, Atlanta, GA.
- Ibrahim, M., Biwole, P. H., Wurtz, E., & Achard, P. (2014). A study on the thermal performance of exterior walls covered with a recently patented silica-aerogel-based insulating coating. *Building and Environment*, 81, 112–122. <https://doi.org/10.1016/j.buildenv.2014.06.017>

**VIII. List of symbols**

<b>Symbol</b>	<b>Definition</b>
S/BP	Starch/Beet Pulp
HC	Hemp concrete
D	Diameter (m)
H	Height (m)
L	Length (m)
t	Thickness (m)
A	Exposed area of the test specimen (m <sup>2</sup> )
G	Water vapour flow rate through specimen (Kg/s)
S	Hydraulic diameter of specimen (m)
T	Thermodynamic temperature (K)
$\Delta m_{12}$	Change of mass per time for a single determination with respect to time (Kg/s)
m <sub>1</sub>	Mass of the test assembly at t <sub>1</sub> (Kg)
m <sub>2</sub>	Mass of the test assembly at t <sub>2</sub> (Kg)
m <sub>i</sub>	Initial mass of the specimen (Kg)
m <sub>t</sub>	Mass of the specimen at time t (Kg)
t <sub>1</sub> and t <sub>2</sub>	Successive time of weighings (s)
G	Mean of five successive determination of $\Delta m_{12}$ for each specimen (kg/s)
g	Density of water vapour flow rate(kg/(m <sup>2</sup> .s))
W	Corrected vapour permeance (kg/(m <sup>2</sup> .s.Pa))
Z	Water vapour resistance ((m <sup>2</sup> .s.Pa)/Kg)
d	specimen thickness (m)
d <sub>a</sub>	Thickness of air layer (m)
$\delta_a$	Water vapour permeability of air (kg/(m.s.Pa))
$\delta$	Water vapour permeability of specimen (kg/(m.s.Pa))
$\Delta p_v$	Water vapour pressure difference across specimen (Pa)
P <sub>sat</sub>	Water vapour saturation pressure (Pa)
S <sub>d</sub>	Water vapour diffusion-equivalent air layer thickness (m)
$\mu$	Water vapour resistance factor

Aw	Capillary absorption coefficient ( $\text{Kg}/(\text{m}^2 \cdot \text{S}^{0.5})$ )
Wlt	Long-term water absorption by total immersion (volume %)
Wf	Free saturation by total immersion ( $\text{kg}/\text{m}^3$ )
V	Volume of the test specimen ( $\text{m}^3$ )
$\rho_w$	Density of water ( $\text{kg}/\text{m}^3$ )
$\rho$	Bulk density ( $\text{kg}/\text{m}^3$ )
c	Specific heat ( $\text{J}/(\text{kg} \cdot \text{K})$ )
Hw	Enthalpy of water ( $\text{J}/\text{m}^3$ )
$\theta$	Temperature ( $^{\circ}\text{C}$ )
$\lambda$	Thermal conductivity ( $\text{W}/(\text{m} \cdot \text{K})$ )
hv	Latent heat of evaporation ( $\text{J}/\text{kg}$ )
$\phi$	Relative humidity (%)
w	Moisture content ( $\text{kg}/\text{m}^3$ )
DI	Liquid diffusivity ( $\text{m}^2/\text{s}$ ).
ACH	Air change per hour ( $\text{h}^{-1}$ )
TWC	Total water content ( $\text{Kg}/\text{m}^2$ )
DR	Dryness rate (%)
CR	Condensation Risk (%)
$\omega$	Time lag (h)
f	Decrement factor
MGR	Mould growth rate ( $\text{mm}/\text{year}$ )
MI	Mould index (-)